Cancer Research

Evolution of Cancer Stem-like Cells in Endocrine-Resistant Metastatic Breast Cancers Is Mediated by Stromal Microvesicles

Pasquale Sansone[1], Marjan Berishaj[1], Vinagolu K. Rajasekhar[1], Claudio Ceccarelli[2], Qing Chang[1], Antonio Strillacci[1,3], Claudia Savini[1,2,4], Lauren Shapiro[5], Robert L. Bowman[6], Chiara Mastroleo[1], Sabrina De Carolis[2,4], Laura Daly[1], Alberto Benito-Martin[7], Fabiana Perna[8], Nicola Fabbri[9], John H. Healey[9], Enzo Spisni[3], Monica Cricca[2], David Lyden[7,10,11], Massimiliano Bonafé[2,4], and Jacqueline Bromberg[1,12]

Abstract

The hypothesis that microvesicle-mediated miRNA transfer converts noncancer stem cells into cancer stem cells (CSC) leading to therapy resistance remains poorly investigated. Here we provide direct evidence supporting this hypothesis, by demonstrating how microvesicles derived from cancer-associated fibroblasts (CAF) transfer miR-221 to promote hormonal therapy resistance (HTR) in models of luminal breast cancer. We determined that CAF-derived microvesicles horizontally transferred miR-221 to tumor cells and, in combination with hormone therapy, activated an ER^{lo}/$Notch^{hi}$ feed-forward loop responsible for the generation of $CD133^{hi}$ CSCs. Importantly, microvesicles from patients with HTR metastatic disease expressed high levels of miR-221. We further determined that the IL6–pStat3 pathway promoted the biogenesis of onco-miR-221^{hi} CAF microvesicles and established stromal CSC niches in experimental and patient-derived breast cancer models. Coinjection of patient-derived CAFs from bone metastases led to *de novo* HTR tumors, which was reversed with IL6R blockade. Finally, we generated patient-derived xenograft (PDX) models from patient-derived HTR bone metastases and analyzed tumor cells, stroma, and microvesicles. Murine and human CAFs were enriched in HTR tumors expressing high levels of $CD133^{hi}$ cells. Depletion of murine CAFs from PDX restored sensitivity to HT, with a concurrent reduction of $CD133^{hi}$ CSCs. Conversely, in models of $CD133^{neg}$, HT-sensitive cancer cells, both murine and human CAFs promoted *de novo* HT resistance via the generation of $CD133^{hi}$ CSCs that expressed low levels of estrogen receptor alpha. Overall, our results illuminate how microvesicle-mediated horizontal transfer of genetic material from host stromal cells to cancer cells triggers the evolution of therapy-resistant metastases, with potentially broad implications for their control. *Cancer Res; 77(8); 1927–41. ©2017 AACR.*

Introduction

Tumor heterogeneity and resistance to therapy may occur from microvesicle-mediated transfer of genetic material between cells (1–3). Thus, the characterization of this phenomenon could have important clinical ramifications most notably in the development of new therapeutically relevant compounds.

Although adjuvant hormonal therapy (HT) improves disease-free survival in luminal breast cancer patients, HT-resistant (HTR) metastatic disease commonly develops in the bones of these patients. This observation suggests that the bone microenvironment may foster estrogen receptor (ER)-independent growth of luminal breast cancer leading to HTR metastases.

The interaction of stromal cells (cancer-associated fibroblasts; CAF) with tumor cells has been shown to mediate and modulate estrogen receptor–dependent (e.g., fibronectin, collagen) and independent proliferation (e.g., laminin) of luminal breast cancer cells, suggesting that stroma–tumor communication may play a pivotal role in the ER-independent self-renewal of breast cancers (4). In the metastatic microenvironment, we hypothesize that chronic inflammation incurred by anti-estrogen therapy and the effects of disseminated tumor cells on the local microenvironment will lead to the activation of resident stromal cells or circulating mesenchymal stem cells to become CAFs. Once

[1]Department of Medicine, Memorial Sloan Kettering Cancer Center, New York, New York. [2]Department of Experimental, Diagnostic and Specialty Medicine, AlmaMater Studiorum, Università di Bologna, Bologna, Italy. [3]Department of Biological, Geological and Environmental Sciences, Università di Bologna, Bologna, Italy. [4]Center for Applied Biomedical Research Laboratory, Policlinico Universitario S. Orsola-Malpighi AlmaMater Studiorum, Università di Bologna, Bologna, Italy. [5]Department of Radiation Oncology, Kaiser Permanente, Oakland, California. [6]Cancer Biology and Genetics Program, Memorial Sloan Kettering Cancer Center, New York, New York. [7]Department of Pediatrics, Cell and Developmental Biology, Children's Cancer and Blood Foundation Laboratories, Weill Cornell Medicine, New York, New York. [8]Molecular Pharmacology and Chemistry Program, Memorial Sloan Kettering Cancer Center, New York, New York. [9]Orthopedics Service, Memorial Sloan Kettering Cancer Center, New York, New York. [10]Drukier Institute for Children's Health, Meyer Cancer Center, Weill Cornell Medicine, New York, New York. [11]Department of Pediatrics, Memorial Sloan Kettering Cancer Center, New York, New York. [12]Department of Medicine, Weill Cornell Medicine, New York, New York.

Note: Supplementary data for this article are available at Cancer Research Online (http://cancerres.aacrjournals.org/).

D. Lyden, M. Bonafé, and J. Bromberg contributed equally to this article.

Corresponding Author: Jacqueline Bromberg, Memorial Sloan Kettering Cancer Center, 1275 York Avenue, Box 397, New York, NY 10065. Phone: 646-888-3112; Fax: 646-888-3200; E-mail: bromberj@mskcc.org

doi: 10.1158/0008-5472.CAN-16-2129

activated, the CAFs may sustain a feed-forward circuit of self-renewal, proliferation, and differentiation of CSCs, resulting in metastasis.

As tumors become more metastatic and resistant to targeted therapies, the number and types of CSCs increases, suggesting that CSCs evolve from non-CSC cells in a given tumor niche (5, 6). The role of stroma microvesicles (MV) in the generation of therapy-resistant cancer and the regulation of self-renewal remains poorly investigated.

Here, we investigated the hypothesis that HT- and CAF-derived microvesicles converge to promote HT resistance and ER-independent self-renewal in luminal breast cancer. By employing patient-derived xenografts from breast cancer bone metastases and experimental models of luminal breast cancer, we uncovered a unique process of CAF-mediated resistance to HT. Our data demonstrate the formation of therapy-resistant stromal-tumor niches via an IL6/Stat3-driven expansion of CAFs, CAF-MV–mediated oncomiR-221 transfer to cancer cells leading to the expansion of $Notch3^{hi}/ER^{lo}/CD133^{hi}$ CSCs. These data reinforce the concept of targeting the stromal niche to prevent both HT resistance and metastatic progression (7–9).

Materials and Methods

Microvesicle isolation and *in vivo* education experiment

Plasma (10 mL) was collected and processed within 4 hours from patients with metastatic disease (Supplementary Table S1) and in healthy controls who were consented to an MSKCC biospecimen protocol #12-137. The plasma and conditioned media (CM) from cancer and CAF cultures was collected from 10^7 cells grown in 5 × 10 cm dishes and centrifuged for 20 minutes at 3,000 × *g* at 4°C. The supernatant was subsequently centrifuged for 30 minutes at 12,500 × *g* at 4°C. The supernatant was transferred and centrifuged at 100,000 × *g* for 90 minutes at 4°C. The supernatant was discarded while the pellet, containing microvesicles, was resuspended in 25 mL of PBS and loaded onto a 5 mL 30% sucrose cushion to deplete microvesicles from extracellular proteins (300 g/L sucrose, 24 g/L Tris base, pH 7.4). Samples were centrifuged at 100,000 × *g* for 90 minutes 4°C. Cushion (3.5 mL), containing microvesicles, was diluted with 10 mL of PBS and centrifuged at 100,000 × *g* for 90 minutes at 4°C. The supernatant was discarded and the pellet resuspended in 25 μL of PBS. Microvesicles were treated with 0.1 mg/mL of DNase I solution (Epicentre) to eliminate contaminating DNA bound to the microvesicles surface or present in solution. Nanosight (Lyden laboratory, Cornell Medical Center) and electron microscopy (MSKCC Electron Microscopy Core) were used to characterize the physical structures of these microvesicles (size and distribution). Confocal microscopy (MSKCC Microscopy Core) of cancer cells educated with prelabeled (PKH67-Green Fluorescent Cell Linker Kit, Sigma) CAF-MVs was performed to ensure transfer and uptake. The *in vivo* role of CAF-MVs in the promotion of HT-resistant luminal breast cancer was determined by injecting CAF-MVs (Mu-CAFs, isolated from HT-resistant xenografts and cultured *in vitro*) and control microvesicles (from MCF7 cells) into the arterial circulation (retro-orbital injection, 3 × 10^9 particles/mouse/weekly) of tumor-bearing mice (MCF7 cells). Once mammary fat pad (MFP) xenografts were established (after 4 months), mice were treated with HT (fulvestrant; 100 μg/injection/once a week for 3 months).

Primary cultures and patient-derived xenografts of endocrine-resistant luminal breast cancer bone metastases

Patient-derived xenografts (PDX) were established from $n = 2$ of 5 HT-resistant and 1 *de novo* stage IV breast cancer bone metastatic tissue isolated at MSKCC (Supplementary Table S2). Patients who developed metastatic breast cancer in the bone were enrolled in the study (IRB protocol #97-094). Following surgery, tissue was processed by the pathologist, 60% of the specimen was used for confirmation of diagnosis and molecular analyses (IHC, IMPACT analyses), while 40% was used for further analysis. Tissues were placed in sterile Epicult (Voden Medical), minced with sterile razor blades and incubated at 37°C for 8 to 12 hours in the presence of Collagenase/Hyaluronidase enzyme mix (1,000 Units, Voden Medical). To grow tumor cells devoid of its cognate stroma, we performed serial centrifugations to separate epithelial cells as mammosphere cultures (MS). Secondary and tertiary MS potential (II or III-MS) was performed as follows: 7-day primary MS started to form after 4–6 days, then they were disaggregated in 1× Trypsin-EDTA (StemCell Technologies), washed in complete MEGM, filtered through a 40-μm nylon mesh, and seeded to form second generation MS. Number of MS was assessed by counting the total number of spheres (size > 100 μm) from cells seeded in low-attachment plates (from 100 to 1,000). To establish primary CAF cultures from patient-derived tissue, MS-depleted supernatant was centrifuged at 450 × *g* for 10 minutes; this pellet was enriched with stromal cells was plated onto 10-cm plates supplemented with DMEM 10% serum media. CAF primary cultures were expanded *in vitro* for $n = 10$ passages. III-MS primary cultures were used to establish PDXs: 50–100 MS (size ~100 μm) were injected in the MFP of NOD/SCID mice and tumor growth was determined over a period of 5 months. At the endpoint of the experiment, xenograft tissues were collected and primary PDX cultures were established. Multiple passaged PDX were generated following repeated orthotopic injection of PDX-derived $EpCAM^{pos}$ cancer cells (recognizes only human cells) in the MFPs of NOD/SCID mice (from 1st to 4th generation). Luminal breast cancer cells expressing a vector for GFP/Luciferase were generated and used for all the *in vivo* experiments. Tumor growth was determined using *in vivo* bioluminescence technology (BLI: Xenogen, IVIS System). Luminal cancer xenografts from the coinjection of human CAFs and MCF7 cells were also generated to determine the effect of the stroma on the generation of *de novo*–resistant endocrine tumors

Xenograft assays and preclinical trials

All cancer cell lines were engineered to express a GFP-positive luciferase expression vector. Prior to *in vivo* inoculation, cancer cells were FACS purified (for GFP) and injected bilaterally in the MFPs of 5- to 7-week-old NOD/SCID) mice (obtained from NCI, Frederick, MD). For each *in vivo* experiment, cancer cells were mixed with an equal volume of Matrigel (BD Biosciences) in a total volume of 50 μL. Bioluminescence was used to monitor both tumour growth (weekly) and metastatic burden (at necropsy). Luminal cancer xenografts from the coinjection of human CAFs (HTR bone metastases) and MCF7 cells (10^3 cells) were also generated to determine the effect of the stroma on the generation of *de novo*–resistant endocrine tumors. In addition, human bone marrow stromal cells HS27a, HS27shC, and HS27shIL6 (100 cells/injection) were coinjected with MCF7 cells (10^3 cells/injection) into the MFP. For immunostaining assays, organs were

collected and fixed overnight in 4% paraformaldehyde, washed, embedded in paraffin, and sectioned (Histo-Serve Core). Hematoxylin and eosin (H&E) staining was performed by standard methods. For the detection of metastases at secondary sites, we performed *in vivo* BLI as well as immunofluorescence/IHC staining for GFP and ER. All the surgical procedures and animal care followed the institutional guidelines and an approved protocol from our IACUC at MSKCC. For the preclinical studies, injectable fulvestrant (Faslodex, AstraZeneca) was given intramuscularly in the tibialis posterior/popliteal muscles (100 μg/injection/once a week) for 2 months. Tocilizumab (Actemra, Roche Pharmaceuticals) was diluted in PBS at a final concentration of 20 mg/mL. A dosage of 100 μg/g/mouse was administered intraperitoneally every week (this is ∼5-fold higher than the physiologic range, patients receive 8 mg/kg i.v.). Control mice received isotype control (placebo) or PBS injection.

Cell lines and FACS

Human cancer cell lines (Namalwa, lymphoma; HeLa, cervical carcinoma), human breast cancer cell lines (MCF7, ZR751, T47D, and BT474), human bone marrow stromal cell lines (HS5, HS27a), and human normal fibroblasts (MRC5, HMF) were purchased from the ATCC and authenticated by short tandem repeat (STR) DNA profiling (Genomic Core MSKCC). Murine CAFs (Mu-CAF) were isolated from HTR xenografts and PDXs by FACS purification ($GFP^-/EpCAM^-$). Cells were mycoplasma free and maintained in minimum essential medium and RPMI (ATCC and Media Core) supplemented with 5% FBS (Media Core), 2 mmol/L glutamine, 100 U mL^{-1} penicillin, and 0.1 mg mL^{-1} streptomycin (Media Core). Cancer cells from xenografts were isolated from primary and metastatic tissues by enzymatic digestion (Collagenase/Hyaluronidase, Sigma-Aldrich), sorted ($GFP^+/DAPI^-$), and cultured *in vitro*. The following reagents: 4-hydroxytamoxifen and fulvestrant were purchased from Sigma (Sigma-Aldrich). For FACS/flow analyses, tumors were digested in sterile Epicult media (StemCell Technology), minced with sterile razor blades, and incubated for 3 hours in the presence of collagenase/hyaluronidase (1,000 Units/sample). Cells were washed with sterile filtered PBS supplemented with 1% BSA (PBS-BSA 1%) and filtered through a 40 μm nylon mesh (BD Biosciences). For the detection of CD44 and CD133, EpCAM antigens, cells were stained in a volume of 100 μL (PBS-BSA 1%) with each antibody CD44-APC (100 ng/10^6 –10^8 cells Clone IM7, eBiosciences), CD133/1-PE (100 ng/10^6–10^8 cells, clone AC133, Miltenyi Biotech) and EpCAM-FITC (250 ng/10^6–10^8 cells, Clone VU-1D9, StemCell Technologies). Cells were labeled on ice for 30 minutes and analyzed (BDFACS Aria III, Flow Core). Samples were analyzed for cell population distribution and sorted for GFP/viability ($GFP^+/DAPI^-$) and CD133/CD44 expression. For flow plot analyses, samples were run using FlowJo 7.5 software (Tree Star). shRNAs for Notch3 and IL6 were previously described (10, 11).

Microarray and miRNA analyses

Normalized gene expression values were downloaded from the GEO under accession number GSE17705 and probes were aggregated to median gene level expression. A CAF gene set from Allinen and colleagues (12) was used in a single sample gene set enrichment analysis (ssGSEA). ssGSEA scores were z-scored and a "CAF score" was assigned to each patient. Patients were split at the median into CAF-high and CAF-low groups. PROM1-high and PROM1-low groups were split based on PROM1 (CD133) median expression. Statistical significance for differences in PROM1 expression and ESR1 expression were assessed with a Student *t* test. The heatmap for CAF signature gene and PROM1 was plotted in R with the heatmap.2 function. For real-time PCR (qPCR), we extracted RNA using TRIzol (Invitrogen). RNA concentration was determined with a NanoDrop 2000. For microarray analysis of published datasets, normalized gene expression data were downloaded from the Gene Expression Omnibus (GEO). Each gene was mean centered and scaled by SD. All analyses were conducted in R. Normalized gene expression data was downloaded from the NCBI for dataset GSE69280 (5). For qPCR, 1 μg of total RNA was reverse transcribed to cDNA using iScript Select cDNA Synthesis Kit (Bio-Rad) following the manufacturer's protocol. Reverse transcription PCR (RT-PCR) analysis was performed using the following primers: ERα; forward 5′-TGAAAGTGGGATACGAAAAGAC-3′, reverse 5′-CAGGATCTCTAGCCAGGCACAT-3′; β2μ forward 5′-ACCCCCACTGAAAAAGATGA-3′, reverse 5′-ATCTTCAAACCTCCATGA-3′. DNA was isolated using phenol/chloroform technique from PDX-derived EpCAM-positive/negative cells. The presence of murine and human cells was determined on 2 ng of DNA by PCR for GAPDH (murine: forward 5′-AGCAGCCGCATCTTCTTGTGCAGTG-3′, reverse 5′- GGCCTTGACTGTGCCGTTGAATTT-3′; Human: forward 5′-CTCTGCTCCTCCTGTTCGAC-3′, reverse 5′- ACGACCAAATCCGTTGACTC-3′). miRNA expression was analyzed as described previously (13). Briefly, miRNA were reverse transcribed using stem-loop RT-PCR technology (14) and amplified by real-time PCR using SYBR Select Master Mix (Applied Biosystems) and ViiA 7 Real-Time PCR System (Applied Biosystems) according to the manufacturer's instructions. The melting curve data were collected to check PCR specificity. miRNA expression was normalized against RNA U6 levels: (RT-miR-221) 5′-GTCGTATCCAGTGCAGGGTCCGAGGTATTCGCACTGGATACGACGAAACCC-3′; (RT-miR-222) 5′-GTCGTATCCAGTGCAGGGTCCGAGGTATTCGCACTGGATACGACACCCAGT-3′; (RT-miR-101) 5′-GTCGTATCCAGTGCAGGGTCCGAGGTATTCGCACTGGATACGACTTCAGTT-3′; (forward-miR-221) 5′-AGCTACATTGTCTGCTGGGTTTC-3′; (forward miR-222) 5′-AGCTACATCTGGCTACTGGGT-3′; (forward miR-101) 5′-GCCGCTACAGTACTGTGA-3′; (forward U6) 5′-CTTCGGCAGCACATATACT-3′; (reverse U6) 5′-AAAATATGGAACGCTTCACG-3′ (reverse all miRs) 5′-TGCAGGGTCCGAGGTAT-3′. All primers were purchased from Eurofins MWG Operon. miRNA expression was analyzed as described elsewhere (13).

Protein and *in vitro* studies

For immunoblotting assays, cells were lysed in buffer (50 mmol/L Tris at pH 7.5, 150 mmol/L NaCl, 5 μg/mL aprotinin, pepstatin, 1% NP-40, 1 mmol/L EDTA, 0.25% deoxycholate, and protease inhibitor cocktail tablet, Sigma). Proteins were separated by SDS-PAGE, transferred to polyvinylidene difluoride membranes and blotted with specific antibodies (Supplementary Table S3). For functional interference studies, anti-miR-221 and control RNA oligonucleotide were purchased from Applied Biosystems. MCF7 cells were seeded in a 6-well plate (8×10^5 cells/well) at 60% confluence. After 24 hours, cells were transfected using Lipofectamine 2000 transfection reagent (Invitrogen) according to the manufacturer's instructions (RNA final concentration, 200 nmol/L). After 6 hours of

incubation at 37°C, transfection medium was replaced with 2 mL of complete medium containing 10% FCS supplemented with/without CAF-MVs. For determination of cell viability, we seeded 2,500 cells per well in 96-well plates and treated them with fulvestrant (10 μmol/L). Viable cells were determined 7–14 days after treatment using Trypan blue and cell counting was done using bright-field microscopy or DAPI staining by flow cytometry (Dako Cytomation). Crystal violet assay was performed to obtain information of the relative cell density at the endpoint of proliferation potential experiments. IL6 ELISA assays were performed using the conditioned medium collected from 5-day cultures of CAF-derived cells seeded at 2×10^6 cells/plate. Proliferation assay was carried out using CalceinAM technology (Invitrogen): cells were seeded in 96-well plates treated with the prefluorescent compound for 20 minutes and fluorescence was read using a plate reader (SpectraMax plate platform). To determine the selective growth potential of cancer cells over stroma cells, we analyzed the proliferation potential of luciferase-positive cancer cells by *in vitro* BLI: cells were seeded in 96-well plates in presence/absence of distinct CAFs/normal fibroblast (1:10 ratio of CAFs to tumor cells) and treated with fulvestrant (10 μmol/L/weekly for 3 weeks). Luciferase activity was measured weekly. Cytokine Arrays were performed on 10 μg of CM-derived proteins according to manufacturer's protocol (Antibody Array 3, RayBiotech. Inc.).

Immunostaining analysis

Serial sections of formalin-fixed paraffin-embedded samples were immunostained using monoclonal anti-CD133 diluted 1:70 (clone W6B3C1, Miltenyi Biotec), anti-ERα RTU (clone SP1, Ventana), anti-Pankeratin RTU (clone AE1/AE3/PCK26, Ventana), and polyclonal anti-Notch-3 diluted 1:400 (M-134, Santa Cruz Biotechnology). CD133 and Notch3 immunostaining was performed as follows: sections were dewaxed, rehydrated, and subjected to antigen retrieval treatment. Antigens were unmasked with a Tris-EDTA pH 9.0 buffer at 98°C for 20 minutes in a waterbath. Endogenous peroxidase activity was inhibited using a 0.5% H_2O_2 solution in methanol for 20 minutes at room temperature. Sections were processed using a non-biotin–amplified method (Novolink, Novocastra) according to the manufacturer's protocols. When mouse tissue was used, a short treatment (30 minutes at room temperature) with MOM blocking solution (Vector Laboratories Inc.) was conducted prior to primary antibody overnight incubation at 4°C. The reaction was visualized using the UltraView DAB Detection System. The immunologic reaction was developed using a 3,3′-diaminobenzidine (DAB)/H_2O_2 PBS pH 7.2–7.4 solution for 10 minutes. Sections were then washed in distilled water and counterstained in Harris hematoxylin. Anti-ERα (ER) and Pankeratin (CK) immunostaining was performed on an automated immunostainer (Benchmark Ultra, Ventana) using the UltraView DAB Detection kit according to the manufacturer's protocol. Antigen retrieval was performed onboard with UltraCC1 buffer (pH 8.2–8.5) at 95°C for 52 minutes (ER) or 20 minutes (CK). Primary antibodies were incubated 28 minutes at 37°C (ER) or 8 minutes at room temperature (CK). For CD133 and Notch3 evaluation, each section was examined at 400×. In each microscopic field, the neoplastic cells were classified according to both positive percentage and staining intensity: [percentage = 0 if <1%, 1 if >1% < 25%, 2 if >25% < 50%, 3 if >50% <75%, 4 if >75%; intensity = 1 (weak), 2 (moderate), and 3 (strong)]. A final classification was obtained by multiplying the two mean values (percentage and intensity, IRS score). As for ER evaluation, the neoplastic population was scanned using Image Cytometry and reported as percentage of positive cells (%) (IMAGE-Pro Plus V5.0.1, Media Cybernetics Inc.). A detailed histologic examination of xenograft tissues was performed at the collaborating institution (University of Bologna, Bologna, Italy). Xenograft tissue was stained with hematoxylin and eosin and examined by three independent pathologists (C. Ceccarelli, Donatella Santini, and M. Bonafe, from the University Hospital of Bologna, Bologna, Italy). For each microscope field (200×), the area occupied from cancer cells, stromal cells, and necrotic components was evaluated and represented as percentage.

Characterization of CAFs

Serial sections (5 μm) of paraformaldehyde-fixed paraffin-embedded samples underwent antigen retrieval using Leica Bond ER2 Buffer (Leica Biosystems) for 20 minutes at 100°C before staining with 1 μg/mL Desmin rabbit polyclonal antibody (Abcam catalog no. ab8592) and 1 μg/mL pStat3 (clone D3A7, Cell Signaling Technology) for 1 hour using Leica Protocol F (Molecular Imaging Core facility, MSKCC, New York, NY). Quantification of Desmin/pStat3 staining was performed using ImageJ/FIJI (NIH, Bethesda, MD). At least 19 fields at 400× were randomly selected and evaluated. The results were expressed as percentage of immunostained cells/over total area of tissue. To discriminate between cancer and stromal cells, fortified H&E staining was also performed (HistoServ Inc). A color deconvolution algorithm was then used, with RGB vectors for the stromal component and counterstain/background stain created from regions of interest drawn from example images (Molecular Imaging Core facility, MSKCC, New York, NY). Appropriate thresholds were then set for each cell type of interest and area measurements were taken for all images. To rule out possible non-CAFs/noncancer cells component, specific staining for CAFs (desmin-murine CAFs) and cancer cells (human pankeratin) was also performed in serial section slides. Stroma–tumor niches were evaluated as area of tissue slide with the copresence of pankeratin-positive cells and stroma cells.

ALDEFLUOR assay

ALDEFLUOR analysis was performed using the ALDEFLUOR Kit (StemCell Technologies) according to the manufacturer's protocol. Cancer cells from PDX primary cultures were washed with 5 mL 10% PBS supplemented with Accumax (Innovative Cell Technologies), and single-cell suspensions were first stained with anti-CD133-PE–conjugated antibody for 20 minutes, washed twice with PBS-BSA (5%), and then incubated with ALDEFLUOR reagent.

CM preparation and phenotypic assays

CM was isolated from CAFs and cancer cell lines (10^8 cells), concentrated using Amicon Ultra-15 centrifuge tubes (Millipore), and protein levels were measured by the Lowry technique; 10 μg of total extracellular protein was loaded for zymographic/protein (MMP-2, MMP-9) and *in vitro* studies (invasion capacity). Cell growth of cocultured cancer cells with CAFs was determined with

and without anti-Jagged1/Notch3 blocking antibody (AF1277, R&D Systems 500 ng every 72 hours). Briefly, luciferase-positive breast cancer cells (MCF7) grown with CAFs (1:50) were seeded in 96-well plate and treated with fulvestrant (10 μmol/L/weekly) in the presence of mouse anti-Jagged1 blocking antibody. BLI signals were measured every 48 hours and growth curves were generated accordingly.

Luciferase assays

Cells were plated in 6-well plates at a density of 2×10^5 cells per well. Cells were transfected with 0.3 μg of promoter luciferase (*CD133*; ref. 15) and the activated form of *Notch3* (pNICD3 2 μg; ref. 10). To normalize transfection efficiency, cells were also cotransfected with 0.1 μg of the pRL-CMV (*Renilla* luciferase, Promega). Forty-eight hours after transfection, luciferase activity was measured using the Dual-Luciferase Assay Kit (Promega). Three independent experiments were performed, and the calculated means and SDs are presented.

TaqMan gene expression profile and RT-PCR

qPCR was performed on 100 ng of cDNA using TaqMan precustom probes (Applied Biosystems, ERα Hs00174860 62 pb, GATA3 Hs00231122 80 bp, FOXA1 Hs0418755 59 bp, GREB1 Hs00536409 67 bp, EGR3 Hs00231780 91 bp, CCL5 Hs00174575 63 bp, PGR Hs01556702 77 bp) and SYBR Green technique (α-sma forward 5′- CAGGGCTGTTTTCCCATCCAT-3′, reverse 5′-GCCATGTTCTATCGGGTACTTC-3′; SDF-1α forward 5′-CCATGAACGCCAAGGTCGTG-3′, reverse 5′- CCAGGTACTCCTGAATCCAC-3′; Vimentin forward 5′-TGGCACGTCTTGACCTTGAAA-3′, reverse 5′- GGTCATCGTGATGCTGAGAA -3′; Slug 5′-AGATGCATATTC GGACCCACA-3′, reverse 5′- CCTCATGTTTGTGCAGGAGA-3′; CD44 forward 5′-CAGCAACCCTACTGATGATGACG-3′, reverse 5′- GCCAAGAGGGATGCCAAGATGA -3′). ViiATM 7 Real-Time PCR System was used (Applied Biosystems) in accordance with the manufacturer's instructions. For analysis, ΔC_t method was applied and fold change was calculated ($2^{-\Delta\Delta C_t}$). All values were normalized to GAPDH expression (TaqMan, Hs02758991). RT-PCR for Notch3 (forward 5′-TCAGGCTCTCACCCTTGG-3′, reverse 5′-AGTCACTGGCACGGTTGTAG-3′), Jagged1 (forward 5′-TCGCTGTATCTGTCCACCTG-3′, reverse 5′-AGTCACTGGCACGGTTGTAG-3′) and β2μ as internal control 5′-ACCCCCACTGAAAAAGATGA-3′, reverse 5′-ATCTTCAAACCTCCATGA-3′ was performed in MCF7 cells control and shNotch3 and mCAFs/fibroblast cell lines.

Statistical analysis

Statistical analysis was performed by SPSS (SPSS Inc.). Continuous variables were analyzed by unequal variance *t* test, paired *t* test (samples, $n = 2$), general linear model (GLM) ANOVA, or GLM for repeated measures (samples, $n > 2$). Mann–Whitney and Wilcoxon tests were used to analyze ordinal variables. *P* values were adjusted for multiple comparisons according to Bonferroni correction. Association among quantitative variables was quantified by Pearson correlation coefficient. Categorical variables were analyzed by Monte Carlo χ^2 test. All the tests were two-sided. $P < 0.05$ was considered significant. Elda software was used to measure the statistics of limiting dilution experiments (bioinf.wehi.edu.au/<http://bioinf.wehi.edu.au/>software/elda/).

Results

Microvesicles from CAF-mediated HT resistance

The presence of CAFs have been assessed as prognosticators in breast cancer and an "active stromal signature" in normal fibroblasts exhibits a tumor-promoting phenotype (16). Many stromal-secreted factors including IL6, SFD-1α, and HFG participate in the communication between CAFs and tumor cells within the tumor microenvironment.

Stromal microvesicles have also been implicated in tumor progression in glioblastomas and ovarian cancers (17, 18). However, the molecular and pathologic relevance of CAF-derived microvesicles in luminal breast cancer remains unclear.

To study tumor progression in luminal breast cancer, we established long-term xenografts of highly tumorigenic MCF7 and ZR751 cells (5). Following tumor establishment (1 cm), all mice received HT (fulvestrant a selective estrogen receptor degrader commonly given to patients with ER^+ metastatic disease, 10 μmol/L) for 3 months. Although the majority of xenografts displayed sensitivity to HT (HTS, stable disease or remission), approximately 10% of the xenografts (data not shown) grew in the presence of therapy (Fig. 1A, HTR resistance to HT). Interestingly, the histologic analysis of these tissues revealed the enrichment of CAFs in the HTR xenografts (Fig. 1B; Supplementary Fig. S1A). Furthermore, we could isolate and *in vitro* passage CAFs from HTR-derived xenograft tissues. These CAF cell lines displayed the upregulation of CAF markers by Western blot analysis and the capability of growth for multi passages (more than 20 passages; Fig. 1B and data not shown). Although we were able to isolate CAFs from HTS lesions in a small fraction of xenografts (5%, $n = 3$ out of 60), we could not propagate them in culture for more than 2 passages (2 weeks). Therefore, no CAF cell lines (0%) were established from HTS xenografts.

To further characterize these tumor-associated stromal cells, we cultured HTR tumors and isolated stromal cells by FACS (negative selection with EpCAM, which recognizes epithelial cells) and determined that $EpCAM^{neg}$ cells were morphologically spindle shaped, were murine in origin (expressed murine genomic DNA, data not shown) and expressed markers of activated CAFs including Fap, vimentin, fibronectin, and activated Stat3 (Fig. 1B, phospho tyrosine 705 Stat3 pStat3).

Next, we asked whether these CAFs could promote *de novo* HTR disease. We cocultured murine CAFs and human-HS27a "CAF" like cells (bone marrow–derived immortalized mesenchymal cells) with HT ($Luciferase^{pos}$) naïve cancer cells in the presence/absence of HT (fulvestrant, 10 μmol/L/weekly) and cancer cell growth was analyzed by *in vitro* bioluminescence after 2 weeks (Fig. 1C). We found that CAFs promoted tumor cell growth following HT, whereas no difference was found in the absence of therapy (Fig. 1D; Supplementary Fig. S1B). In contrast to HS27a cells and murine CAFs, normal fibroblasts (mammary and lung) did not confer resistance to HT in cocultures (Supplementary Fig. S1C).

In addition to growth factors, stromal cells have been shown to secrete microvesicles, which can horizontally transfer numerous prosurvival factors and confer resistance to radiotherapy (19). Here we determined that the number of microvesicles produced by murine CAFs and HS27a cells was much greater than MCF7 tumor cells (Fig. 1E). To determine whether these microvesicles could confer a protumorigenic advantage, we set up an *in vivo* model (Fig. 1F). MFP xenografts from HT-naïve cells (MCF7) were

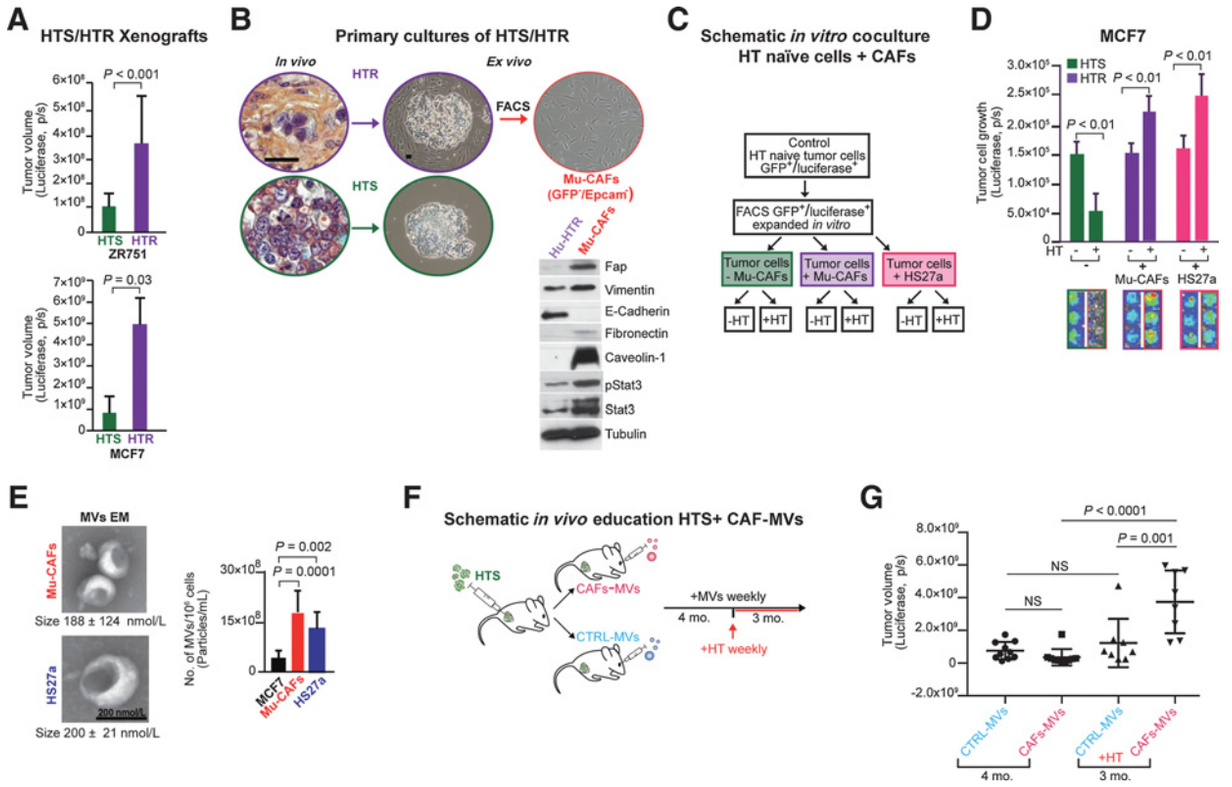

Figure 1.

Microvesicles from CAFs mediated HTR. **A,** Generation of HTR (purple) and HTS (green) xenografts in luminal breast cancer. Highly tumorigenic luminal breast cancer cells (MCF7 and ZR751 luciferase positive) were injected in the MFP; xenograft-bearing mice were treated with fulvestrant starting at 4 months for 3 months (HT, fulvestrant intramuscular injection 100 μg/mouse/weekly). Some tumors grew in the presence of HT (HTR), while the majority of them was sensitive to HT (HTS). Data reported as error bars mean bioluminescence (BLI value ± SEM) at the endpoint of the experiment (7 months, $n = 10$ mice/group). **B,** HTR cultures were enriched with murine CAFs (Mu-CAFs, red). Representative fortified H&E staining of HTR xenografts (from **A**, MCF7, scale bar, 50 μm; yellow, stroma desmoplastic reaction), bright-field images of primary cultures from HTS and HTR xenografts and Western blot analysis of FACS-purified cancer cells (Hu-HTR) and murine cells (Mu-CAFs). **C,** Schematic of the experiment. HT-naïve cancer cells (GFP^+/$luciferase^+$) were cocultured with FACS purified Mu-CAFs (purple), human BMSC/CAF HS27a cells (red), or in the absence of stromal cells (green). Cells were treated with or without HT (fulvestrant, 10 μmol/L/weekly). **D**, Proliferation potential (after 2 weeks, BLI) was determined ±HT (fulvestrant, 10 μmol/L). Data are reported as error bars, mean ± SD of $n = 3$ independent experiments. *, $P < 0.05$ (Student t test). **E**, Electron microscopy images and quantification (number by nanosight) of CAF-derived microvesicles (murine and human, HS27a). Scale bar, 200 nm; data reported as error bars, mean ± SD of number of particles/mL for 10^6 cells. *, $P < 0.05$ (Student t test) of $n = 3$ independent experiments. **F,** Schematic of the experiment. Mice were injected in the MFP with HTS cells (MCF7) and subsequently injected weekly with either Mu-CAFs microvesicles or control microvesicles (MCF7 derived; see Materials and Methods). After 4 months, HT was administered for 3 months (fulvestrant intramuscular injection 100 μg/mouse/weekly). **G,** Dot plot of tumor growth of HTS cells (luciferase/p/s) grown in the MFP of mice educated with CAF MVs or CTRL MVs (MCF7) in the presence/absence of HT (fulvestrant, see **F**; microvesicles, retro-orbital injection, 3×10^9 particles/mouse/weekly); error bars, mean ± SEM of the last point of the growth curve before (4 months) and after HT (7 months). *, $P < 0.05$ values refer two-way ANOVA (**G**). NS, not significant.

established; CAF-MVs (3×10^9) and control microvesicles (tumor-derived microvesicles, MCF7) were injected retro-orbitally weekly for 7 months. Once tumors were established (after 4 months) all mice received HT (fulvestrant weekly). Although there was no difference in tumor growth before HT, those animals treated with CAF-MVs had tumors resistant to HT (HTR) while MCF7-MVs provided no benefit as tumors regressed with HT (Fig. 1G). Overall, these data demonstrated that circulating stromal microvesicles can induce resistance to HT *in vivo*.

CAF-derived microvesicle transfer of oncomiR-221/222 to cancer cells promotes *de novo* HT resistance

Distinct genes and pathways have been associated with resistance to HT including the activation of mutations in the *ESR1* gene (20), increased Her2 expression (21), decreased ER levels, and ER transcriptional signatures (22, 23), increased expression of oncomiRs including the ER repressor miR-221/222 (24) and, more recently, increased Notch signaling in CSCs (5, 25).

As a reduction in ER expression is associated with resistance to HT (22), and $CD133^{hi}$ CSCs have lower ER levels (mRNA and protein) as compared with $CD133^{lo}/CD44^{lo}$ cells, we reasoned that the suppression of ER signaling could be a mechanism of stroma-mediated expansion of therapy-resistant CSCs ($CD133^{hi}/Notch3^{hi}$).

To test our hypothesis, we first demonstrated that the CM from CAFs (murine and human), but not normal fibroblasts, led to a decrease in ER protein expression and ER-dependent transcripts (e.g., GATA3, FOXA1, GREB1, EGR3, CCL5, PGR) in MCF7 cells (Fig. 2A; Supplementary Fig. S2A). As the

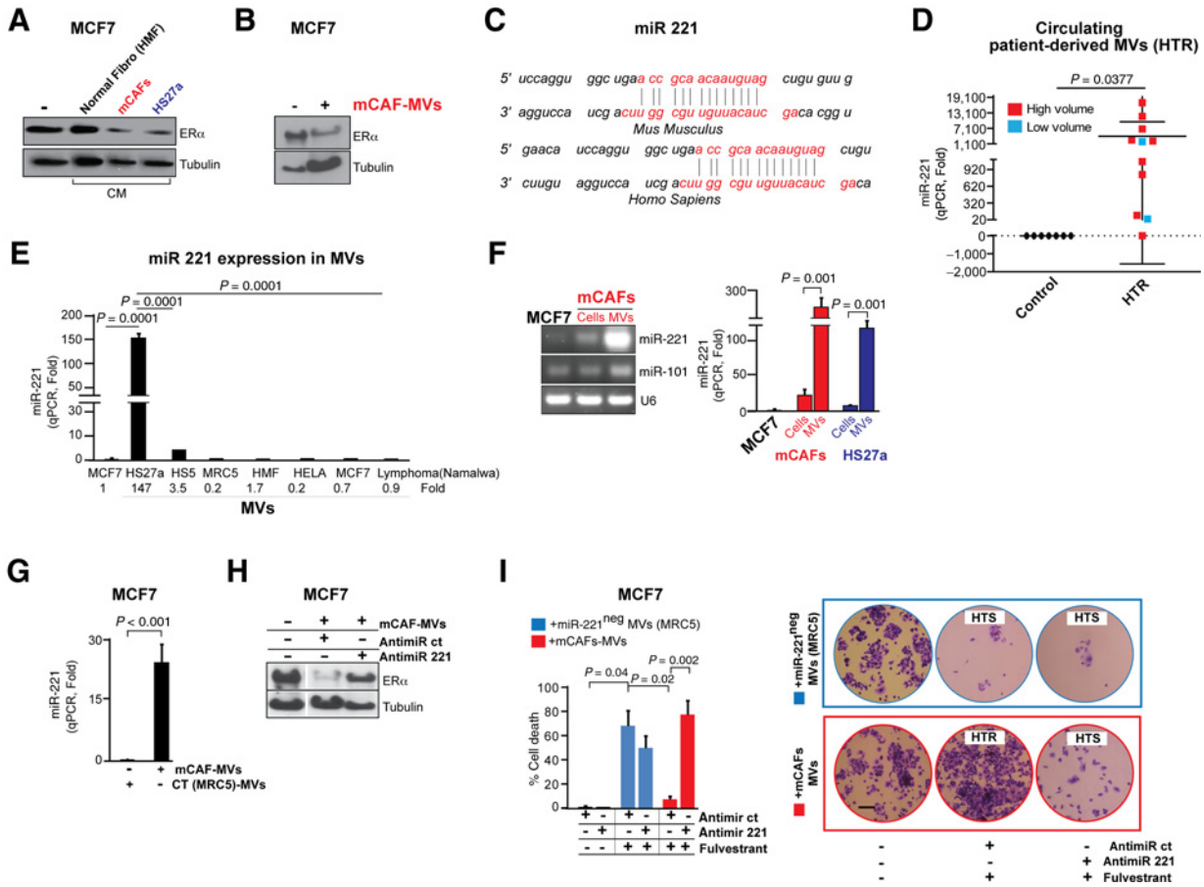

Figure 2.

Microvesicle-mediated OncomiR-221 transfer from CAFs to cancer cells promotes an ER^{lo} phenotype, leading to HTR resistance **A**, Western blot analysis of ERα protein in MCF7 cells following treatment with the CM of human normal mammary fibroblasts (HMF), mCAFs (red font), and HS27a cells (blue font, 48 hours). **B**, Western blot of ERα protein in MCF7 cells treated with and without mCAF-derived microvesicles (10^8 particles, 48 hours). **C,** Image showing the OncomiR-221 sequence conservation in *Mus Musculus* and *Homo Sapiens*. **D,** MV-miR221 expression as determined by qPCR as fold increase from patients with HTR disease and healthy controls (reference MCF7-MVs was used and normalized to total RNA expression, $n = 3$ replicates; Supplementary Table S1). Patients with high volume disease (>10% of organ involvement) are denoted in red and low volume disease (<1% of organ involvement) is denoted in blue. **E,** Bar graphs representing oncomiR-221 expression (qPCR) in microvesicles from indicated sources (10^8 cells). Data are reported as fold increase (221/U6 expression) ± SD of $n = 3$ replicates (MV-MCF7 is used as reference). **F,** RT-PCR analysis of miR-221 and 101 in MCF7, mCAFs, and mCAF-derived microvesicles (RNA was isolated from 10^{15} particles) and bar graph showing oncomiR-221 expression (qPCR, Fold, normalized to U6 values) in mCAFs and HS27a cells and their respective microvesicles. The expression of oncomiR-221 in MCF7 was used as a reference control. **G,** Bar graph of oncomiR-221 (qPCR, Fold) in MCF7 cells following chronic mCAF-MV education (one month, 10^8 particles weekly). Microvesicles were isolated from MRC5 cells (normal lung fibroblasts) and used as control microvesicles (CT-MVs). **H,** Western blot analysis of ERα protein in MCF7 cells treated with mCAF-MVs (10^8 particles, 48 hours) previously transfected (24 hours before microvesicle education) with the anti-miR-221 or control (CT; see Materials and Methods); **I,** Bar graph representing cell death (by Trypan blue, %) of MCF7 cells transfected with anti-miR-221 and controls, treated with fulvestrant (10 μmol/L, 7 days) in the presence/absence of mCAF and MRC5 microvesicles (10^8 particles every 48 hours). miR-221–negative microvesicles were used as control microvesicles and were obtained from normal lung fibroblasts (MRC5). Representative images of Crystal violet staining of MCF7 cells at the endpoint of the experiment described in **H**. Data are reported as mean ± SD of three independent experiments ($n = 3$). NS, not significant. *P* values, Student *t* test (**D–G**, **I**).

suppression of ER protein occurred with CM from both murine and human CAFs, we hypothesized that rather than soluble factors (which can be typically species-specific; refs. 26, 27), CAF-derived miRNAs might be mediating the downregulation of ER expression. Microvesicles have been suggested to be mediators of nucleic acid transfer including miRNAs (27). Among different miRNAs, the forced overexpression of oncomiR-221/222 in luminal breast cancer cells has been found to reduce ER expression and promote HT resistance (24). In addition, increased plasma levels of miR-221 were found in ER-negative breast cancer patients (28). The administration of 10^8 microvesicles from mCAFs to ER$^+$ cancer cells (MCF7) reduced ER levels after 48 hours (Fig. 2B). We showed that oncomiR-221/222 sequences are conserved between human and mouse species, suggesting possible functional cross-species interactions (Fig. 2C). Importantly, miR-221 expression was found in circulating microvesicles from patients with HTR metastatic disease (independent of tumor burden) as compared with healthy controls (Fig. 2D, $n = 11$; Supplementary Table S1).

We determined that CAF-derived microvesicles were enriched for miR-221 compared with normal fibroblasts and distinct cancer cells lines (breast, cervical, and lymphoma),

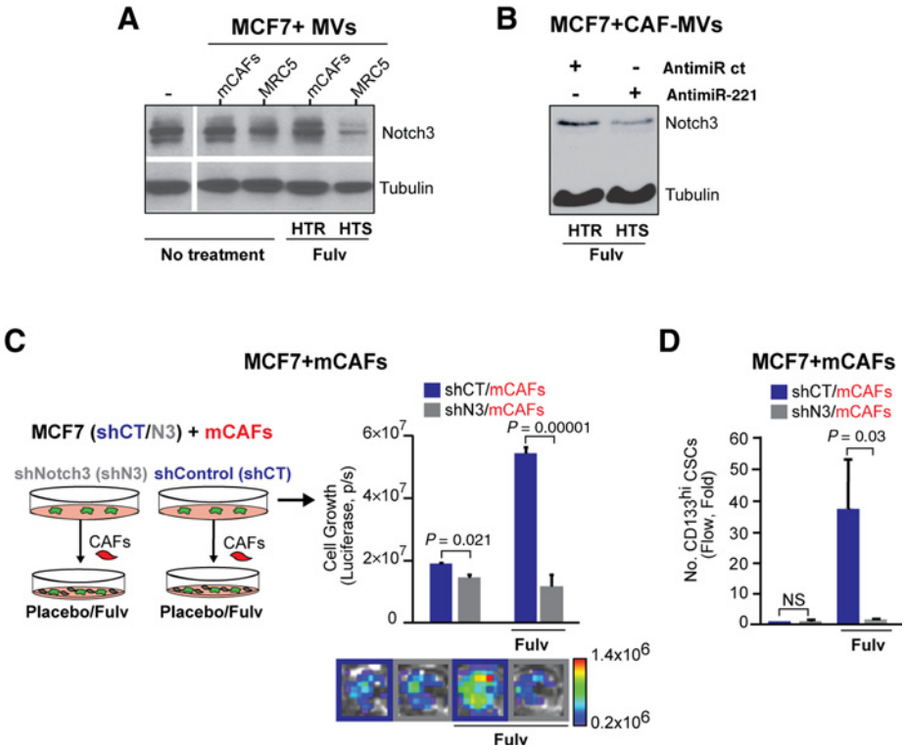

Figure 3.

CAF-mediated expansion of CD133^{hi} CSCs via an OncomiR-221^{hi}/ER^{lo}/Notch3^{hi}loop. **A,** Western blot analysis of Notch3 protein from MCF7 cells in the presence/absence of mCAF and MRC5 microvesicles (10^8 particles every 48 hours) ± fulvestrant (Fulv; 10 μmol/L for 7 days). Tubulin was used as a loading control. **B,** Representative Western blot analysis of Notch3 protein from MCF7 cells transfected with the anti-miR-221/CT (1 μg/well) and treated with fulvestrant and mCAF-MVs (48 hours). Tubulin was used as a loading control. **C,** Schematic of coculture experiments. Control (shCT) and Notch3 knocked-down MCF7 GFP/Luciferase$^+$ cells (shN3) were cultured with PDX-derived mCAFs (1:10; mCAFs:cancer cells) in the presence/absence of fulvestrant (Fulv, 10 μmol/L, weekly administration for a month); growth of MCF7 shCT/shN3 cells in cocultures was then determined. Data are reported as mean (luciferase, p/s -photons/seconds-) ± SEM of the last time point of the growth curve or 28 days (three biological replicates with three technical replicates each). **D,** Fold Increase in CD133^{hi} CSCs (flow analysis) from MCF7 shCT/shN3 cell cocultures treated with fulvestrant (1 month, endpoint, **C**). Data are reported as total number of CD133-positive cells (mean ± SD of fold change) of $n = 3$ different specimens (as a reference, total numbers of CD133^{hi} cells from 10^9 naïve MCF7 cells were used). NS, not significant. *P* values, Student *t* test (**C**, **D**).

suggesting that stroma-derived microvesicle could account for the increased level of miR-221 expression in microvesicles (Fig. 2E). Accordingly, miR-221, but not a control miRNA (miR-101), was highly expressed (100- to 200-fold enrichment) in microvesicles from CAFs as compared with microvesicles from normal fibroblasts, CAFs and cancer-derived cell lines (Fig. 2F; Supplementary Fig. S2B). Administration of murine CAF-MVs compared with normal fibroblast-MVs (MRC5) to MCF7 cells (oncomiR-221 negative) led to the transfer of oncomiR-221 (Fig. 2G, 20-fold increase in expression in educated cancer cells).

To address the consequences of microvesicle-derived oncomiR-221 transfer in mediating HT resistance, anti-miR-221 was transfected in cancer cells before microvesicle administration. We demonstrated that anti-miR-221 transfection abrogated mCAF-MV–dependent downregulation of ER protein (Fig. 2H) and HT resistance following chronic mCAF-MV education (Fig. 2I). Restored sensitivity to HT in anti-miR-221–transfected cells was associated with an increase in ER expression/activity (Supplementary Fig. S2C and S2D). These data suggest that CAF–microvesicle–mediated HT resistance occurs via the transfer of onco-miR-221 promoting an ER^{lo} phenotype.

CAF-mediated expansion of CD133^{hi} CSCs via an oncomiR-221^{hi}/ER^{lo}/Notch3^{hi}loop

Increased expression of Notch and downstream signaling events as well as a higher number of CSCs are found in HT-resistant breast cancer (29, 30). Among Notch proteins, Notch3 and Notch4 are crucial mediators of resistance to HT in distinct models of luminal breast cancers (5, 25, 31, 32).

Given the pivotal role of CAF-derived microvesicle in promoting the switch from sensitive to resistant disease (HTS to HTR), we asked whether these stromal microvesicles could also modulate Notch3 expression. We cultured MCF7 cells with fulvestrant (10 μmol/L/weekly) for 2 weeks (see schematic Fig. 1C) with microvesicles (10^8 particles/weekly) from either MRC5 or mCAFs. Although no effect was observed in the absence of HT (no treatment), mCAF-MVs restored Notch3 expression and activity (Hes1, Hey 1 mRNAs) following fulvestrant, which associated with increased growth (Fig. 3A; Supplementary Fig. S3A, HTR cells see Fig. 2I). Conversely, MRC5-MVs administered cells did not overcome ER-dependent downregulation of Notch3 expression and activity (Hes1, Hey 1 mRNAs) as well as the suppression of growth (Fig. 3A, for HTS cells, see Fig. 2I). The transfection of anti-miR-221 led to decreased Notch3 protein levels and restored

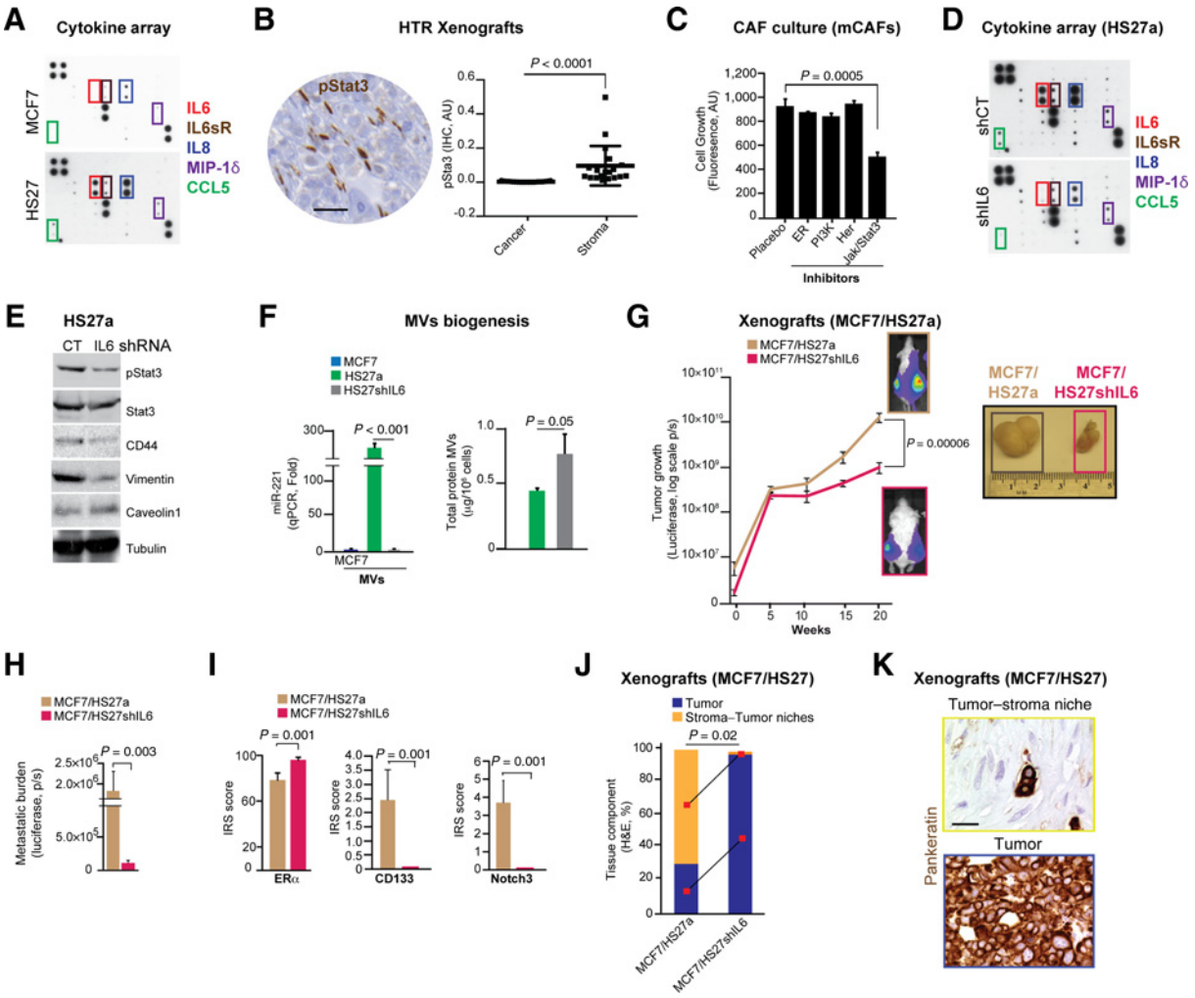

Figure 4.

IL6/Stat3 signaling from CAFs promotes the expansion of CD133^{hi} CSCs. **A,** Cytokine array expression of the CM from MCF7 and HS27a cells (10 μg total protein). Highlighted are overexpressed cytokines and chemokines (IL6, IL6sR, IL8, MIP-1δ, and CCL5). **B,** Dot plot showing phospho-tyrosine 705 Stat3 (pStat3) IHC quantification in HTR-derived primary tumor tissues (see Fig. 1B) in both the stroma and tumor compartments. Quantification of pStat3 was performed using ImageJ/FIJI (NIH) of $n = 19$ fields from $n = 5$ different tumors. The results were expressed as ratio of pStat3 IHC value/total tissue area. A representative IHC image is shown. Scale bar, 25 μm. **C,** Bar graph of the proliferation capacity (Calcein AM, fluorescence) of xenograft-derived mCAFs isolated from HTR xenografts (Fig. 1) and cultured in the presence of vehicle (placebo) or signaling pathway inhibitors including ER (fulvestrant, 10 μmol/L) or PI3K (BYL, 100 nmol/L), HER (lapatinib, 100 nmol/L) or JAK/pStat3 (AZD1480, 500 nmol/L). Data are reported as mean (fluorescence) ± SEM of the last time point of the growth curve (14 days; three biological replicates with three technical replicates each). **D,** Cytokine array expression from the CM (10 μg) of HS27shIL6 versus HS27a cells. Highlighted are overexpressed cytokines and chemokines (IL6, IL6sR, IL8, MIP-1δ, and CCL5). **E,** Western blot analysis of pStat3, Stat3, CD44, vimentin, caveolin1, and tubulin protein levels in HS27a cells CT and shIL6. **F,** Bar graph of OncomiR-221 expression in microvesicles derived from 10^8 HS27a and HS27shIL6 cells (qPCR, fold as reference, MCF7 microvesicles were used, normalized to U6 expression). Bar graph of protein levels (μg) in 10^8 microvesicles isolated from HS27a and HS27shIL6 cells is also shown. **G** and **H,** Tumor growth and metastatic burden (luciferase, BLI) in MCF7/HS27a and MCF7/HS27shIL6 xenografts. 10^3 cancer cells were inoculated in both 4th inguinal MFP with 10^2 HS27a cells (CT or shIL6). Tumor growth was examined over 20 weeks. Data are reported as mean BLI value ± SEM (log scale) for each time point ($n = 4/5$ mice/group). Metastatic burden is mean BLI value ± SEM of signal from metastatic tissues including lymph nodes, lungs, and bones. A representative image of primary tumors from MCF7/HS27a versus MCF7/HS27shIL6 is shown. **I,** Bar graph representing immunohistochemical quantification (IRS score) of ERα, CD133, and Notch3 in tumor-derived tissues from MCF7/HS27a or MCF7/HS27shIL6 xenografts (**G**). Data are reported as mean ± SD of $n = 10$ tissue sections for each group. **J,** Bar graph showing percentage (H&E, %) of stroma–tumor niches versus tumor compartment in primary tumor tissues derived from MCF7/HS27a and MCF7/HS27shIL6 xenografts (**G**). **K,** Representative Pankeratin staining of tissues slides from **G** depicting stroma–tumor niches (cancer cells surrounded by stromal cells). Data are reported as mean ± SD of $n = 10$ tissue slides for each group. *P* values, *t* test (**B**, **F**, **H**, **I**), Wilcoxon two-sample test (**J**), multiple comparisons corrected *post hoc t* test after GLM ANOVA (**C**), repeated measures GLM ANOVA (**G**).

sensitivity to HT (fulvestrant) of CAF-MV–treated cancer cells (Figs. 2I and 3B). These data demonstrate that miR-221 in CAF-MVs can block HT-mediated downregulation of Notch3 expression.

We recently described the enrichment of CD133^{hi}/ER^{lo}/Notch3^{hi} CSCs in HT-resistant tumors, which also expressed high levels of Notch-regulated genes such as *Hey1* and *Hes1* (GSE69280; ref. 5).

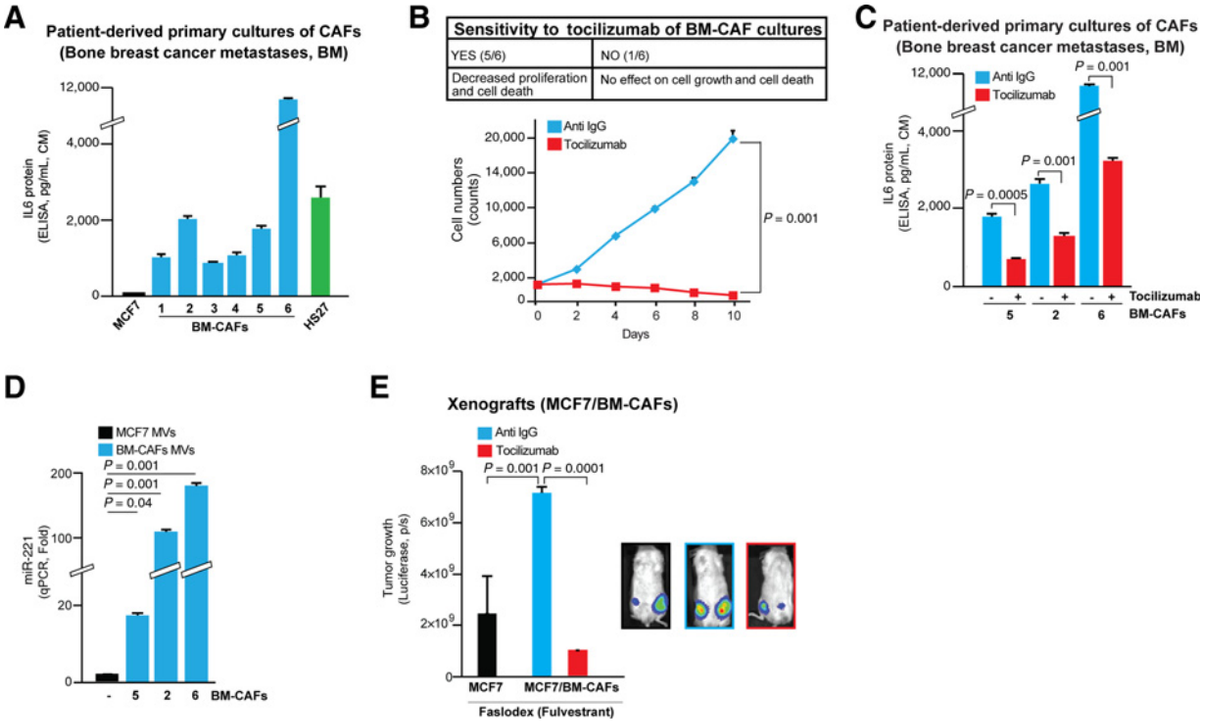

Figure 5.

Autocrine CAF-derived IL6 triggers endocrine-resistant disease. **A,** Bar graph showing IL6 levels measured by ELISA from the CM (10 μg total protein) of primary CAF cultures (BM-CAFs) isolated from patient bone–derived breast cancer metastases (Supplementary Table S2). IL6 levels from MCF7 and HS27a are also shown. **B,** Growth (cell number) of BM-CAFs (specimen 5, Supplementary Table S2) treated with an anti IL6-IL6R antibody tocilizumab (500 ng/mL every 48 hours) versus IgG control. **C,** Bar graph of IL6 protein (ELISA) from the CM (2 μg total protein) of BM-CAFs treated with tocilizumab or IgG for a week (500 ng/mL every 48 hours). **D,** Bar graph of oncomiR-221 expression by qPCR (Fold, normalized on U6 level) in microvesicles isolated from BM-CAF cultures. Microvesicles isolated from MCF7 cells were used as a reference control. **E,** Tumor burden (luciferase) of MCF7 xenografts alone (black) and coinjected with BM-CAFs (specimen 6, Supplementary Table S2) treated with fulvestrant and tocilizumab. Briefly, MCF7 xenografts were established in the MFP of NOD/SCID mice alone (10^3 cells) or in combination with CAFs (10^2 cells). When tumors reached ~1 cm (3 months), mice were randomized ($n = 4$/group) to receive either fulvestrant (1 mg/weekly) or fulvestrant and tocilizumab (100 μg/g/mouse) for 4 months. Data are reported as mean BLI value ± SEM at the endpoint of the experiment (7 months). Data are reported as mean ± SD of three independent experiments ($n = 3$). *P* values, Student *t* test (**C**, **D**, **E**), multiple comparisons corrected *post hoc t* test after repeated measures GLM ANOVA (**B**).

Given the role of CAF or stromal microvesicles in promoting a miR-221^{hi}/ER^{lo}/Notch3^{hi} phenotype, we tested the hypothesis that CAFs could promote the *in vivo* expansion of CD133^{hi} cells via Notch3 upregulation. The selective reduction of Notch3 expression in cancer cells (shNotch3) and activity (using an anti-Jagged1 blocking antibody) abrogated CAF-mediated HT resistance and the expansion of CD133^{hi} cancer cells (Fig. 3C and D; Supplementary Fig. S3B). In agreement with the knockdown experiment, overexpression of the activated form of Notch3 (pNICD3) in MCF7 cells led to an increase in CD133 promoter luciferase activity (pCD133) with HT (fulvestrant) in association with a reduction in ER protein levels (Supplementary Fig. S3C and S3D). These data suggest that higher Notch3 activation could promote a feed-forward ER^{lo}/CD133^{hi} loop necessary for the generation of CD133^{hi} CSCs (Supplementary Fig. S3C and S3D). Overall, our data describe a novel mechanism of HT resistance: CAF-MV–mediated transfer of the onco-miR-221 leading to reduced ER expression and Notch3 upregulation.

IL6/Stat3 activity is required for CAF–CSC niche formation

As the biogenesis of oncomiR-221/222^{hi} microvesicles occurs preferentially in CAFs (not normal fibroblasts), we hypothesized that the abrogation of a CAF phenotype would interfere with the generation of HT-resistant CSCs. To investigate this hypothesis, we examined possible candidates responsible for CAF growth. Compared with breast cancer cells, the CM of CAFs (HS27a cells) expressed higher levels of chemokines (e.g., IL8, MIP-1δ, CCL5) and cytokines, including IL6 an activator of Stat3 (Fig. 4A). These findings were further supported by evidence of high pStat3 levels in murine CAFs from HTR-derived xenografts (Fig. 4B). Differently from other signaling pathways (HER, PI3K, ER), pStat3 activity was required for CAF proliferation as well as the generation of oncomiR-221^{hi} microvesicles (Fig. 4C; Supplementary Fig. S4A). In concordance with these data, reduced IL6 expression in HS27a cells (using an IL6-shRNA) lowered secreted IL8/IL6R/CCL5 levels as well as the expression of CAF markers including pStat3, vimentin, and CD44 (Fig. 4D and E). In addition, compared with HS27shCT cells, HS27shIL6 cells had reduced proliferative and invasive potential (Supplementary Fig. S4B and S4C) as well as lowered MMP2/9 expression and activity, indicating a loss of characteristic CAF features (Supplementary Fig. S4D). Moreover, microvesicles from HS27shIL6 cells had essentially no expression of oncomiR-221 compared with

HS27shCT cells with no change in microvesicle production (Fig. 4F, protein content as a surrogate marker of microvesicle yield). These data suggest that IL6/pStat3 signaling is crucial for the proliferation of CAFs and the production of oncomiR-221$^+$ microvesicles.

To address the phenotypic consequences of decreasing IL6 signaling in CAFs, we coinjected MCF7 cells with HS27shCT and HS27shIL6 CAFs into the MFP of mice. Compared with controls (MCF7/HS27a), the coinjection of MCF7/HS27shIL6 cells resulted in impaired tumor growth, lower metastatic burden, and decreased expression of CD133^{hi}/Notch3^{hi}/ERα^{lo} CSCs (Fig. 4G–I; Supplementary Fig. S4E). In agreement with the loss of CD133^{hi}/Notch3^{hi} CSCs, MCF7/HS27shIL6–derived tumors had fewer stroma–tumor niches (Fig. 4J and K) and decreased pStat3 expression (Supplementary Fig. S4F). Overall, our data suggest that IL6-mediated generation of stromal niches is required for the expansion of CD133^{hi} CSCs.

Anti-IL6 therapy abrogates CAF-mediated *de novo* resistance to HT

To extend our results to clinical specimens, we established primary cultures of stromal cells from patient-derived bone metastases (Supplementary Table S2, BM-CAFs). IL6 is a well-known pleiotropic cytokine, secreted at high levels from the bone marrow microenvironment and CAFs (33, 34). We isolated and cultured CAFs from bone metastases (Supplementary Fig. S5A and data not shown) and detected high levels of IL6 protein from the CM of these primary cultures (Fig. 5A). These levels are similar to those found from the CM of HS27a cells. Consistent with the HS27 model, the abrogation of IL6 signaling, using the anti-IL6R-IL6 antibody (tocilizumab), abrogated the growth in 70% of CAF primary cultures (Fig. 5B), reduced IL6 secretion and the expression of CAF markers (Fig. 5C; Supplementary Fig. S5B), this finding suggests that autocrine IL6 maintains the CAF phenotype of these cells.

Although miR-221/222 expression is very low in luminal breast cancer tissues and cells (Fig. 2), high levels of miR-221 was found in circulating microvesicles from HTR patients (Fig. 2D). Next, we reasoned that, in agreement with other investigators, CAFs would be the major source of miR-221 (35). We then isolated microvesicles from CAF primary cultures derived from bone metastases and found increased levels of oncomiR-221 as compared with tumor microvesicles (Fig. 5D); these results were similar to those found in HS27a cells and mCAFs (Fig. 4). We subsequently demonstrated that the coinjection of BM-CAFs with MCF7 cells promoted HTR tumor growth (treated with fulvestrant) in an IL6-dependent manner, as combination fulvestrant/tocilizumab abrogated tumor growth (Fig. 5E).

CAF-mediated expansion of CD133^{hi} CSCs

We and others have recently demonstrated the enrichment of CSCs expressing CD133 or ALDH^{hi} activity in experimental luminal breast cancers following HT (5, 25). In addition, expression of Prominin1 (CD133) was identified in tumors from patients who progressed on adjuvant HT (23). In agreement with other investigators, CD133^{hi} and CD44^{hi} cells are functionally CSCs as they were capable of engrafting with low cell numbers (<1,000, Supplementary Fig. S6A). We previously demonstrated that differently from CD44^{hi} cells, CD133^{hi}/CD44^{lo} cells expressed embryonic stem cell signatures and increased the expression of ABCG2, a CSC gene associated with therapy resistance (GSE69280; refs. 5, 36). Here we determined that CD133^{hi}/CD44^{lo} cells expressed normal stem cell signatures by GSEA (Supplementary Fig. S6B, GSE69280; ref. 5). In addition, compared with CD133^{lo}/CD44^{lo} and CD44^{hi}/CD133^{lo} cells, the injection of CD133^{hi}/CD44^{lo} cells gave rise to slow-growing tumors (Supplementary Fig. S6C) with an increased capacity to disseminate to the bone marrow (Supplementary Fig. S6D). These data suggest that the CD133^{hi} phenotype is a distinct CSC population (37).

Next, we investigated the hypothesis that extrinsic (stromal heterogeneity) factors could regulate the evolution of therapy-resistant niches leading to metastatic progression (38, 39). We demonstrated high PROM1 (encoding CD133) expression by microarray (GSE17705) was associated with increased levels of a mammary CAF gene signature (12) in the setting of human HT-resistant primary tumors (Fig. 6A, $P < 1.82 \times 10^{-4}$; Supplementary Fig. S7A).

To examine the importance of CD133^{hi} cells in clinically relevant models of metastatic breast cancer, we generated PDXs from HT-resistant (HTR) luminal breast cancer bone metastases (Fig. 6B; Supplementary Table S2). Cultured tumor cells were serially transplanted into the MFP of immunocompromised mice in the presence of HT (fulvestrant: a selective estrogen receptor degrader). After three sequential passages, the enhanced tumorigenic capacity (% tumor take) of PDXs was associated with increased Notch3 expression (Supplementary Fig. S7B), enrichment of CD133^{hi} (∼40-fold) cancer cells and murine stromal cells (∼30 fold), which had infiltrated the tumor (Fig. 6B and C; Supplementary Fig. S7C and S7D). We further determined that the PDX-derived CD133^{hi} cells had low ALDH activity, suggesting different and unique stem cell populations arising through a stroma-mediated metastatic transition within ER$^+$ breast cancer (Supplementary Fig. S7E).

Given the coenrichment of CD133^{hi} cells with CAFs, we hypothesized that CAFs could directly promote the expansion of HT-resistant CD133^{hi} cells. To address this hypothesis, we depleted HT-resistant PDX primary cultures from CAFs (by FACS for EpCAM^{pos}) and maintained these cancer cells in culture for several months. When long-term depleted for murine CAFs, EpCAM^{pos} cells from PDX primary cultures were growth inhibited by HT as compared with tumor cells freshly isolated from cocultures (sorting for EpCAM^{pos}, Fig. 6D and E). Moreover, acquired sensitivity to HT resulted in decreased numbers of self-renewing CD133^{hi} cells (Fig. 6E and F).

To determine whether CAFs could confer *de novo* HT resistance and promote the biogenesis of CD133^{hi} cells, we cultured HT-sensitive MCF7 cells with murine CAFs, isolated from xenografts, with/without HT (fulvestrant) for 4 weeks (Fig. 6G). When cultured with CAFs, MCF7 cancer cells became resistant to HT (fulvestrant), as compared with MCF7 cells alone (Fig. 6G). Concomitant with HTR cancer cell growth, by FACS we observed a marked (30-fold) increase in CD133^{hi} CSCs as compared with MCF7 cells alone (Fig. 6H). Further characterization of the CD133^{hi} cells revealed that ERα mRNA levels were lower in these cells than in CD133^{lo}/CD44^{lo} cells (Fig. 6I). In agreement with these data, higher CD133/PROM1 expression was associated with decreased ESR1 mRNA expression and activity in HT-resistant primary tumors (Fig. 6J, $P < 0.0001$). Overall, these findings demonstrate that CAFs, in the presence of HT, can promote the *de novo* formation of CD133^{hi} CSCs and HTR disease.

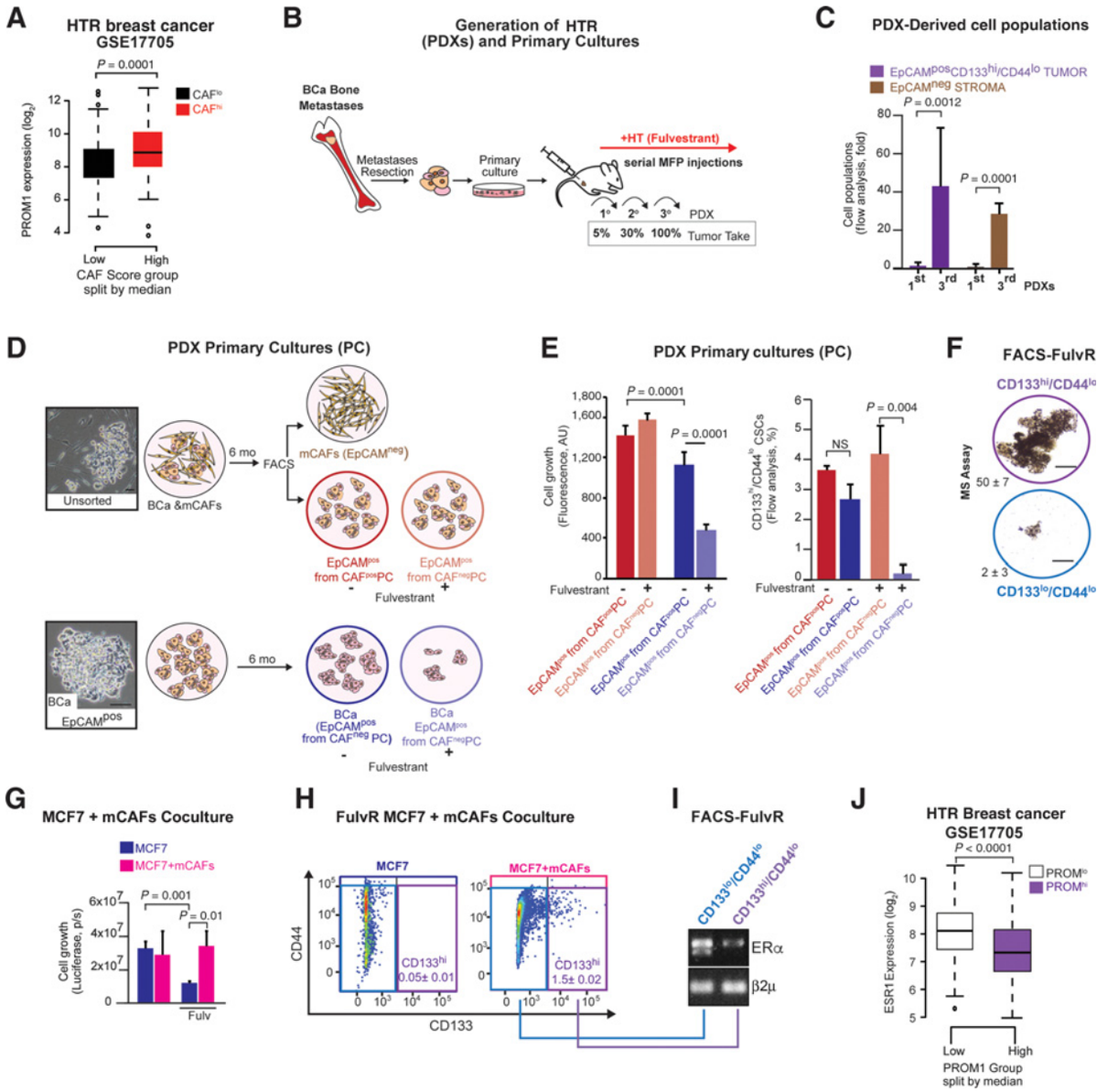

Figure 6.

CAF-mediated expansion of CD133^{hi} CSCs in patient-derived xenografts from HTR breast cancer bone metastases. **A,** Box plot of PROM1 expression (log_2) separated into "low" (black) and "high" (red) groups by the median CAF score as described in Materials and Methods using the GSE17705 dataset (23). Box plots are drawn such that horizontal lines indicate the sample median, the box spanning the interquartile distance (IQD), whiskers extending to 1.5× IQD, and remaining outlying points shown as open circles. **B,** Tumor take percentage (%) of PDXs following three sequential passages *in vivo*. Briefly, cancer cells were isolated from bone metastases (Supplementary Table S2, sample shown B-Met3), grown in culture dishes for 2 weeks and then injected into the MFP of NOD/SCID mice (1st $n = 1/5$; 2nd $n = 3/10$; 3rd $n = 40/40$) treated with HT (fulvestrant, 1 mg/weekly). After 5 months, tumor tissues were digested and cancer cells were cultured *in vitro* and FACS-sorted for EpCAM positivity (to eliminate murine cells) before reinoculating (10^5 EpCAM^{pos} cells) these into new cohorts of mice. **C,** Number of CD133^{hi}/CD44^{lo} cancer cells (EpCAM^{pos}) and stroma cells (EpCAM^{neg}) derived from 1st and 3rd generation PDXs (flow analysis, fold). **D,** Schematic of the *in vitro* PDX culture established in presence/absence of CAFs (CAF^{pos} or CAF^{neg}). Unsorted (cancer cells and CAFs) or previously FACS-purified EpCAM^{pos} cancer cells from PDX primary cultures were grown for 6 months (6 mo), then EpCAM^{pos} cancer cells were FACS-purified from EpCAM^{neg} cells and treated with fulvestrant (Fulv, 10 μmol/L 14 days). Scale bar, 10 μm. **E,** Bar graphs of cell growth (Calcein AM, left panel). Data are reported as mean (fluorescence) ± SEM after 14 days (three biological replicates with three technical replicates each). The number of CD133^{hi} cells (flow analysis, %, right) is also shown after 14 days of culturing. **F,** Images and quantification of secondary MS growth of FACS purified CD133^{hi} and CD133^{lo} cancer cells from experiment **E**. Scale bar, 100 μm. **G,** Schematic and growth of MCF7 (GFP$^+$/luciferase$^+$) cells, using BLI-luciferase grown with and without mCAFs (PDX derived). A 1:10 mCAF to MCF7 cell ratio in the presence/absence of fulvestrant (Fulv, 10 μmol/L, added weekly for 30 days). **H,** Representative CD133/CD44 expression by flow analysis of fulvestrant-resistant MCF7 cancer cells (FulvR) in the presence/absence of mCAFs at the endpoint of the experiment described in **G**. **I,** RT-PCR analysis of ERα in FACS isolated CD133^{hi} and CD133^{lo} cancer cells from experiment panels **G** and **H**. β2μ used as a loading control is shown. **J,** Box plot depicting ESR1 expression (log_2) separated into "low" (white) and "high" (purple) groups by the median *PROM1* expression using the GSE17705 dataset (23). Box plots are drawn with a horizontal line indicating the sample median, box spanning IQD, whiskers extending to 1.5× IQD, and outlying points shown as open circles. Data are reported as mean ± SD of three independent experiments ($n = 3$). *P* values, Monte Carlo χ^2 test (**A**), Student *t* test (**B**, **C**, **E**, **J**), *t* test after GLM ANOVA (**G**), GLM ANOVA for repeated measures (**E**, left).

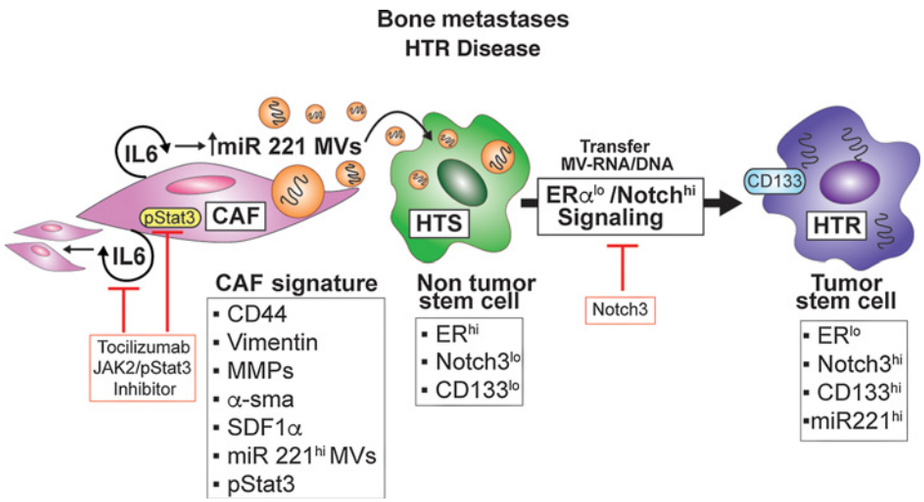

Figure 7.
Stroma microvesicle–mediated CSC evolution in endocrine-resistant metastatic breast cancer. Schematic of the proposed model of CAF-mediated endocrine-resistant disease in luminal breast cancer. Autocrine IL6/Stat3 signaling drives the proliferation of CAFs and the biogenesis of oncomiR-221/222^{hi} microvesicles; these microvesicles are taken up by ER^{pos} breast cancer cells and in conjunction with HT leads to the potent suppression of ER signaling promoting Notch3 upregulation, which in turn sustains the self-renewal of CD133^{hi} CSCs in an ER-independent manner.

In summary, our data led us to propose the following model: IL6 upregulation drives a CAF phenotype leading to the generation of stroma–tumor niches *in vivo*. The presence of active CAFs promotes a skewing of the cancer cell population toward a CD133^{hi}/Notch3^{hi}/ER^{lo} CSC phenotype. This occurs via the production/action of CAF-derived microvesicle, which reduces ER activity leading to HTR disease (Fig. 7; ref. 40).

Discussion

Significant progress has been made in identifying tumor cell–specific factors (e.g., tumor secretome and gene signatures) that promote cancer cell survival and proliferation in the bone microenvironment (27, 41). In addition, cross-talk between bone marrow–derived myeloid cells, osteoclasts, and osteoblasts with tumor cells has identified many growth factors, chemokines, and miRNAs as critical regulators of bone metastasis (42). A recent manuscript by Luo and colleagues has also demonstrated that increased osteoblast-derived IL6 promotes tumor cell seeding and bone metastases in a model of breast cancer cells injected in the arterial circulation (43). IL6 is a pleiotropic cytokine, which is secreted from several cell types, including CAFs and plays a crucial role in the expansion of cancer stem cells (44, 45) as well as in the proliferation potential of CAFs (46, 47).

The presence of CAFs have been assessed as a poor prognostic feature in breast cancer (48) and an "active stromal signature" in normal fibroblasts exhibits a tumor-promoting phenotype (16). Moreover, PDX tumor tissue was shown to be enriched with host CAFs (49); but the molecular and pathologic relevance of any given CAF^{hi} phenotype in PDXs remains unclear.

The majority of breast cancers (~70%) are of the ER-positive or luminal subtype. Although, the suppression of ER activity with HTs has led to improved survival, when these cancers recur they preferentially metastasize to the bone, and eventually acquire resistance to HT and are thus incurable (50, 51).

The upregulation of distinct pathways, including Her2, PI3K, and/or overactive estrogen signaling, are found in metastatic cancer cells escaping tumor dormancy from adjuvant HT. Although targeting these pathways in the metastatic setting leads to clinical responses (52), resistance to anti-Her2/estrogens/PI3K regimens invariably occurs (27, 53). We and others have reported the clinical relevance of high numbers of CD133^{hi} cells in "therapy"-resistant cancers including lung cancer and HT-resistant luminal breast cancer metastases (5, 54).

Recently a crucial role for stromal microvesicle in tumor progression has been suggested (18, 19). However, whether CAF-MVs could promote therapy resistant breast cancer and whether these microvesicles could recapitulate the phenotypic role of CAFs in the tumor microenvironment remain under debate.

Although HT itself suppresses ER signaling, HT alone cannot be a unique trigger of metastatic disease in luminal breast cancer. We propose that communication between CAFs and tumor cells promotes an ER-dependent to an ER-independent switch in metastatic disease. This can occur via the genetic transfer of miRNAs (221/222), leading to the posttranscriptional downregulation of ER and the expansion of HT-resistant tumors. Recently, the overexpression of miR-221/222 was demonstrated to promote mammosphere generation in T47D cells. In addition, a manuscript from Shah and colleagues has proved the presence of miR-221–high microvesicles from CAFs (35). However, the phenotypic relevance of these CAF-MVs in the context of HTR disease was not investigated.

In this article, we have demonstrated that the expansion of CD133^{hi} CSCs is functionally associated with the expansion of CAFs in experimental and patient-derived HTR disease. We developed the hypothesis that CAF-derived microvesicles could generate *de novo* HTR disease via a miR-221–mediated conversion of non-CSCs (ER^{hi}) into therapy-resistant CSCs (ER^{lo}). We generated PDX models of luminal breast cancer and isolated CAFs from HTR bone metastases (Supplementary Table S2) and through their analysis uncovered a step-wise process of CAF-MV–mediated HT resistance: the (i) IL6-pStat3–dependent activation of CAFs, (ii) the biogenesis of oncomiR-221/222–high microvesicles, (iii) the transfer of these oncomiRs from CAF-MVs to ER^{hi} cancer cells, (iv) the suppression of ER signaling, Notch3 activation, and the generation of CD133^{hi}/ER^{lo}/Notch^{hi} CSCs.

Given the pivotal role of IL6 in CAF cell growth and the generation of stromal–tumor niches, we identified combination IL6R–IL6 blockade and HT as a therapeutic intervention to abrogate the establishment of stromal–tumor niches and endocrine resistance in metastatic luminal breast cancer (Fig. 7). Taken together, our data suggest a novel pathologic role of stromal IL6 in

luminal breast cancer: the secretion of oncomiR-221/222 high microvesicles leading to the evolution of therapy-resistant stromal–tumor niches. We characterized the cellular components of this stroma–tumor niche: "CD133^{hi} CSCs and CAFs" and determined the molecular machinery responsible for the niche generation: autocrine IL6 in CAFs and CAF-derived microvesicle-dependent downregulation of ER in cancer cells.

Disclosure of Potential Conflicts of Interest

N. Fabbri is a consultant/advisory board member for Illuminoss Medical Inc. No potential conflicts of interest were disclosed for the other authors.

Authors' Contributions

Conception and design: P. Sansone, D. Lyden, J. Bromberg
Development of methodology: P. Sansone, M. Berishaj, C. Savini
Acquisition of data (provided animals, acquired and managed patients, provided facilities, etc.): P. Sansone, M. Berishaj, V.K. Rajasekhar, Q. Chang, A. Strillacci, L. Shapiro, A. Benito-Martin, N. Fabbri, J.H. Healey, J. Bromberg
Analysis and interpretation of data (e.g., statistical analysis, biostatistics, computational analysis): P. Sansone, M. Berishaj, C. Ceccarelli, Q. Chang, A. Strillacci, R. Bowman, C. Mastroleo, F. Perna, E. Spisni, M. Cricca, D. Lyden, M. Bonafé
Writing, review, and/or revision of the manuscript: P. Sansone, V.K. Rajasekhar, L. Shapiro, L. Daly, D. Lyden, M. Bonafé, J. Bromberg
Administrative, technical, or material support (i.e., reporting or organizing data, constructing databases): P. Sansone, M. Berishaj, S.D. Carolis
Study supervision: P. Sansone, D. Lyden, J. Bromberg

Acknowledgments

We are grateful to Mesruh Turkekul, Afsar Barlas, Sho Fujisawa, Romin Yevgeniy (Molecular Cytology Core), and Donatella Santini (Department of Experimental, Diagnostic and Specialty Medicine, University of Bologna, Italy) for advice and technical assistance.

Grant Support

This study is supported by grants from Department of Defense (W81XWH-10-1-1013 to P. Sansone) the NIH (R01: CA87637 to J. Bromberg), Charles and Marjorie Holloway Foundation (J. Bromberg), Sussman Family Fund (J. Bromberg), Lerner Foundation (J. Bromberg), The Beth C. Tortolani Foundation (J. Bromberg and D. Lyden), MSK Cancer Center Support Grant/Core Grant (P30 CA008748 to J. Bromberg), NIH (U01-CA169538 to D. Lyden), The Manning Foundation (D. Lyden), The Hartwell Foundation (D. Lyden), Fundacao para aCiencia e a Tecnologia (D. Lyden), The Nancy C and Daniel P Paduano Foundation (D. Lyden), The Mary Kay Foundation (D. Lyden), Pediatric Oncology Experimental Therapeutic Investigator Consortium (POETIC; D. Lyden), James Paduano Foundation (D. Lyden), Malcolm Hewitt Weiner Foundation (D. Lyden), Theodore A Rapp Foundation (D. Lyden), American Hellenic Educational Progressive Association 5th District Cancer Research Foundation (D. Lyden). C. Savini won a Marco Polo fellowship from the University of Bologna. M. Bonafè is supported by the Cornelia and Roberto Pallotti Legacy.

The costs of publication of this article were defrayed in part by the payment of page charges. This article must therefore be hereby marked *advertisement* in accordance with 18 U.S.C. Section 1734 solely to indicate this fact.

Received August 2, 2016; revised January 12, 2017; accepted January 12, 2017; published OnlineFirst February 15, 2017.

References

1. Yu DD, Wu Y, Shen HY, Lv MM, Chen WX, Zhang XH, et al. Exosomes in development, metastasis and drug resistance of breast cancer. Cancer Sci 2015;106:959–64.
2. Challagundla KB, Wise PM, Neviani P, Chava H, Murtadha M, Xu T, et al. Exosome-mediated transfer of microRNAs within the tumor microenvironment and neuroblastoma resistance to chemotherapy. J Natl Cancer Inst 2015;107:186–91.
3. Nouraee N, Mowla SJ, Calin GA. Tracking miRNAs' footprints in tumor-microenvironment interactions: Insights and implications for targeted cancer therapy. Genes Chromosomes Cancer 2015; 54:335–52.
4. Haslam SZ, Woodward TL.Host microenvironment in breast cancer development: epithelial-cell-stromal-cell interactions and steroid hormone action in normal and cancerous mammary gland. Breast Cancer Res 2003;5:208–15.
5. Sansone P, Ceccarelli C, Berishaj M, Chang Q, Rajasekhar VK, Perna F, et al. Self-renewal of CD133(hi) cells by IL6/Notch3 signalling regulates endocrine resistance in metastatic breast cancer. Nat Commun 2016;7:10442.
6. Dalerba P, Clarke MF. Cancer stem cells and tumor metastasis: first steps into uncharted territory. Cell Stem Cell 2007;1:241–2.
7. Hermann PC, Huber SL, Herrler T, Aicher A, Ellwart JW, Guba M, et al. Distinct populations of cancer stem cells determine tumor growth and metastatic activity in human pancreatic cancer. Cell Stem Cell 2007; 1:313–23.
8. Vermeulen L, de Sousa e Melo F, Richel DJ, Medema JP. The developing cancer stem-cell model: clinical challenges and opportunities. Lancet Oncol 2012;13:e83–9.
9. Borovski T, De Sousa E Melo F, Vermeulen L, Medema JP. Cancer stem cell niche: the place to be. Cancer Res 2011;71:634–9.
10. Sansone P, Storci G, Giovannini C, Pandolfi S, Pianetti S, Taffurelli M, et al. p66Shc/Notch-3 interplay controls self-renewal and hypoxia survival in human stem/progenitor cells of the mammary gland expanded in vitro as mammospheres. Stem Cells 2007;25:807–15.
11. Chang Q, Bournazou E, Sansone P, Berishaj M, Gao SP, Daly L, et al. The IL-6/JAK/Stat3 feed-forward loop drives tumorigenesis and metastasis. Neoplasia 2013;15:848–62.
12. Allinen M, Beroukhim R, Cai L, Brennan C, Lahti-Domenici J, Huang H, et al. Molecular characterization of the tumor microenvironment in breast cancer. Cancer Cell 2004;6:17–32.
13. Strillacci A, Griffoni C, Sansone P, Paterini P, Piazzi G, Lazzarini G, et al. miR-101 downregulation is involved in cyclooxygenase-2 overexpression in human colon cancer cells. Exp Cell Res 2009; 315:1439–47.
14. Chen C, Ridzon DA, Broomer AJ, Zhou Z, Lee DH, Nguyen JT, et al. Real-time quantification of microRNAs by stem-loop RT-PCR. Nucleic Acids Res 2005;33:e179.
15. D'Anello L, Pasquale Sansone, Gianluca Storci, Valentina Mitrugno, Gabriele D'Uva, Pasquale Chieco, et al. Epigenetic control of the basal-like gene expression profile via Interleukin-6 in breast cancer cells. Mol Cancer 2010;9:300.
16. Al-Rakan MA, Colak D, Hendrayani SF, Al-Bakheet A, Al-Mohanna FH, Kaya N, et al. Breast stromal fibroblasts from histologically normal surgical margins are pro-carcinogenic. J Pathol 2013;231:457–65.
17. Au Yeung CL, Co NN, Tsuruga T, Yeung TL, Kwan SY, Leung CS, et al. Exosomal transfer of stroma-derived miR21 confers paclitaxel resistance in ovarian cancer cells through targeting APAF1. Nat Commun 2016;7:11150.
18. Zhang L, Zhang S, Yao J, Lowery FJ, Zhang Q, Huang W-C, et al. Microenvironment-induced PTEN loss by exosomal microRNA primes brain metastasis outgrowth. Nature 2015;527:100–4.
19. Boelens MC, Wu TJ, Nabet BY, Xu B, Qiu Y, Yoon T, et al. Exosome transfer from stromal to breast cancer cells regulates therapy resistance pathways. Cell 2014;159:499–513.
20. Toy W, Shen Y, Won H, Green B, Sakr RA, Will M, et al. ESR1 ligand-binding domain mutations in hormone-resistant breast cancer. Nat Genet 2013;45:1439–45.
21. Osborne CK, Schiff R. Mechanisms of endocrine resistance in breast cancer. Annu Rev Med 2011;62:233–47.
22. Leary AF, Drury S, Detre S, Pancholi S, Lykkesfeldt AE, Martin LA, et al. Lapatinib restores hormone sensitivity with differential effects on estrogen receptor signaling in cell models of human epidermal growth factor receptor 2-negative breast cancer with acquired endocrine resistance. Clin Cancer Res 2010;16:1486–97.

23. Symmans WF, Hatzis C, Sotiriou C, Andre F, Peintinger F, Regitnig P, et al. Genomic index of sensitivity to endocrine therapy for breast cancer. J Clin Oncol 2010;28:4111–9.
24. Rao X, Di Leva G, Li M, Fang F, Devlin C, Hartman-Frey C, et al. MicroRNA-221/222 confers breast cancer fulvestrant resistance by regulating multiple signaling pathways. Oncogene 2011;30:1082–97.
25. Simoes BM, O'Brien CS, Eyre R, Silva A, Yu L, Sarmiento-Castro A, et al. Anti-estrogen resistance in human breast tumors is driven by JAG1-NOTCH4-dependent cancer stem cell activity. Cell Rep 2015; 12:1968–77.
26. Pedersen LG, Castelruiz Y, Jacobsen S, Aasted B. Identification of monoclonal antibodies that cross-react with cytokines from different animal species. Vet Immunol Immunopathol 2002;88:111–122.
27. Zhang XH, Jin X, Malladi S, Zou Y, Wen YH, Brogi E, et al. Selection of bone metastasis seeds by mesenchymal signals in the primary tumor stroma. Cell 2013;154:1060–73.
28. Zhao R, Wu J, Jia W, Gong C, Yu F, Ren Z, et al. Plasma miR-221 as a predictive biomarker for chemoresistance in breast cancer patients who previously received neoadjuvant chemotherapy. Onkologie 2011;34: 675–80.
29. Haughian JM, Pinto MP, Harrell JC, Bliesner BS, Joensuu KM, Dye WW, et al. Maintenance of hormone responsiveness in luminal breast cancers by suppression of Notch. Proc Natl Acad Sci U S A 2012;109: 2742–7.
30. Bergamaschi A, Madak-Erdogan Z, Kim YJ, Choi YL, Lu H, Katzenellenbogen BS. The forkhead transcription factor FOXM1 promotes endocrine resistance and invasiveness in estrogen receptor-positive breast cancer by expansion of stem-like cancer cells. Breast Cancer Res 2014;16:436.
31. Magnani L, Stoeck A, Zhang X, Lánczky A, Mirabella AC, Wang TL, et al. Genome-wide reprogramming of the chromatin landscape underlies endocrine therapy resistance in breast cancer. Proc Natl Acad Sci U S A 2013;110: E1490–9.
32. Lombardo Y, Faronato M, Filipovic A, Vircillo V, Magnani L, Coombes RC. Nicastrin and Notch4 drive endocrine therapy resistance and epithelial to mesenchymal transition in MCF7 breast cancer cells. Breast Cancer Res 2014;16:R62.
33. Karnoub AE, Dash AB, Vo AP, Sullivan A, Brooks MW, Bell GW, et al. Mesenchymal stem cells within tumour stroma promote breast cancer metastasis. Nature 2007;449:557–63.
34. Nagasaki T, Hara M, Nakanishi H, Takahashi H, Sato M, Takeyama H. Interleukin-6 released by colon cancer-associated fibroblasts is critical for tumour angiogenesis: anti-interleukin-6 receptor antibody suppressed angiogenesis and inhibited tumour-stroma interaction. Br J Cancer 2014;110:469–78.
35. Shah SH, Miller P, Garcia-Contreras M, Ao Z, Machlin L, Issa E, et al. Hierarchical paracrine interaction of breast cancer associated fibroblasts with cancer cells via hMAPK-microRNAs to drive ER-negative breast cancer phenotype. Cancer Biol Ther 2015;16:1671–81.
36. Gilani RA, Kazi AA, Shah P, Schech AJ, Chumsri S, Sabnis G, et al. The importance of HER2 signaling in the tumor-initiating cell population in aromatase inhibitor-resistant breast cancer. Breast Cancer Res Treat 2012;135:681–92.
37. Liu S, Cong Y, Wang D, Sun Y, Deng L, Liu Y, et al. Breast cancer stem cells transition between epithelial and mesenchymal states reflective of their normal counterparts. Stem Cell Reports 2014;2:78–91.
38. Calon A, Lonardo E, Berenguer-Llergo A, Espinet E, Hernando-Momblona X, Iglesias M, et al. Stromal gene expression defines poor-prognosis subtypes in colorectal cancer. Nat Genet 2015;47:320–9.
39. Diaz LA Jr, Williams R, Wu J, Kinde I, Hecht JR, Berlin J, et al. The molecular evolution of acquired resistance to targeted EGFR blockade in colorectal cancers. Nature 2012;486:537–40.
40. Sjostrom AE, Sandblad L, Uhlin BE, Wai SN. Membrane vesicle-mediated release of bacterial RNA. Sci Rep 2015;5:15329.
41. Ren G, Esposito M, Kang Y. Bone metastasis and the metastatic niche. J Mol Med 2015;93:1203–12.
42. Esposito M, Kang Y. Targeting tumor-stromal interactions in bone metastasis. Pharmacol Ther 2014;141:222–33.
43. Luo X, Fu Y, Loza AJ, Murali B, Leahy KM, Ruhland MK, et al. Stromal-initiated changes in the bone promote metastatic niche development. Cell Rep 2016;14:82–92.
44. Sansone P, Storci G, Tavolari S, Guarnieri T, Giovannini C, Taffurelli M, et al. IL-6 triggers malignant features in mammospheres from human ductal breast carcinoma and normal mammary gland. J Clin Invest 2007;117:3988–4002.
45. Korkaya H, Kim G-i, Davis A, Malik F, Henry NL, Ithimakin S, et al. Activation of an IL6 inflammatory loop mediates trastuzumab resistance in HER2+ breast cancer by expanding the cancer stem cell population. Mol Cell 2012;47:570–84.
46. Mace TA, Ameen Z, Collins A, Wojcik S, Mair M, Young GS, et al. Pancreatic cancer-associated stellate cells promote differentiation of myeloid-derived suppressor cells in a STAT3-dependent manner. Cancer Res 2013;73:3007–18.
47. Shintani Y, Fujiwara A, Kimura T, Kawamura T, Funaki S, Minami M, et al. IL-6 Secreted from cancer-associated fibroblasts mediates chemoresistance in NSCLC by increasing epithelial-mesenchymal transition signaling. J Thorac Oncol 2016;11:1482–92.
48. Paulsson J, Micke P. Prognostic relevance of cancer-associated fibroblasts in human cancer. Semin Cancer Biol 2014;25:61–8.
49. Cassidy JW, Caldas C, Bruna A. Maintaining tumor heterogeneity in patient-derived tumor xenografts. Cancer Res 2015;75:2963–8.
50. Coleman RClinical features of metastatic bone disease and risk of skeletal morbidity. Clin Cancer Res 2006;12:6243s–6249s.
51. Davies C, Pan H, Godwin J, Gray R, Arriagada R, Raina V, et al. Long-term effects of continuing adjuvant tamoxifen to 10 years versus stopping at 5 years after diagnosis of oestrogen receptor-positive breast cancer: ATLAS, a randomised trial. Lancet 2013;381:805–16.
52. Baselga J, Campone M, Piccart M, Burris HAIII, Rugo HS, Sahmoud T, et al. Everolimus in postmenopausal hormone-receptor-positive advanced breast cancer. N Engl J Med 2012;366:520–9.
53. Arnedos M, Vicier C, Loi S, Lefebvre C, Michiels S, Bonnefoi H, et al. Precision medicine for metastatic breast cancer–limitations and solutions. Nat Rev Clin Oncol 2015;12:693–704.
54. Bertolini G, D'Amico L, Moro M, Landoni E, Perego P, Miceli R, et al. Microenvironment-modulated metastatic CD133+/CXCR4+/EpCAM-lung cancer-initiating cells sustain tumor dissemination and correlate with poor prognosis. Cancer Res 2015;75:3636–49.